

Quantum field theoretical description for the reflectivity of graphene

M. Bordag,¹ G. L. Klimchitskaya,^{2,3} V. M. Mostepanenko,^{2,3} and V. M. Petrov³

¹*Institute for Theoretical Physics, Leipzig University,
Postfach 100920, D-04009, Leipzig, Germany*

²*Central Astronomical Observatory at Pulkovo of the
Russian Academy of Sciences, St.Petersburg, 196140, Russia*

³*Institute of Physics, Nanotechnology and Telecommunications,
St.Petersburg State Polytechnical University, St.Petersburg, 195251, Russia*

Abstract

We derive the polarization tensor of graphene at nonzero temperature in (2+1)-dimensional space-time. The obtained tensor coincides with the previously known one at all Matsubara frequencies, but, in contrast to it, admits analytic continuation to the real frequency axis satisfying all physical requirements. Using the obtained representation for the polarization tensor, we develop quantum field theoretical description for the reflectivity of graphene. The analytic asymptotic expressions for the reflection coefficients and reflectivities at low and high frequencies are derived for both independent polarizations of the electromagnetic field. The dependencies of reflectivities on the frequency and angle of incidence are investigated. Numerical computations using the exact expressions for the polarization tensor are performed and application regions for the analytic asymptotic results are determined.

PACS numbers: 12.20.Ds, 11.10.Kk, 11.10.Wx, 73.22.Pr

I. INTRODUCTION

During the last few years, a two-dimensional sheet of carbon atoms called graphene attracted much experimental and theoretical attention [1]. It is unique material whose electronic excitations at small frequencies below a few eV demonstrate the linear dispersion relation and are described by relativistic quantum electrodynamics [1, 2]. This allows calculation of the reflectivity properties of graphene with respect to incident electromagnetic waves starting from first principles of quantum field theory. In fact, graphene presents the possibility to test at a laboratory table several effects predicted by quantum field theory, which were commonly considered unfeasible for observation in the past due to extreme values of parameters required for their realization. One could mention the interaction of graphene with an electrostatic potential barrier (the Klein paradox) [3] and creation of quasiparticle pairs in graphene either by the Schwinger mechanism in static electric field [4, 5] or in a time-dependent field [6].

Previously, the reflectivity of transverse magnetic (TM), i.e., p polarized, electromagnetic waves on graphene was investigated using the local model for the in-plane (longitudinal) graphene conductivity [7, 8]. Both the transverse magnetic and transverse electric (TE) reflection coefficients (i.e., for both, p and s , polarizations of the electromagnetic field) were expressed in terms of the polarization tensor at zero [9] and nonzero [10] temperature. This approach, entirely based on quantum electrodynamics, was used to calculate the Casimir interaction in different systems involving graphene [9–17] and turned out to be very productive. Specifically, the existence of large thermal effect in the Casimir force for graphene at short separations, discovered in Ref. [18] using the longitudinal density-density correlation function in the random phase approximation, was confirmed and investigated in detail.

It should be taken into account, however, that the temperature-dependent contribution to the polarization tensor found in Ref. [10] is perfectly correct only at the imaginary Matsubara frequencies. The representation of Ref. [10] uses the Feynman parameter and its formal analytic continuation to the whole plane of complex frequency, for instance, to real frequencies, disagrees with that used in general thermal quantum field theory [19]. Thus, the results of Ref. [10] are well adapted to calculate the Casimir force, but are not applicable for the investigation of reflectivity of graphene at real frequencies. As a result, calculations of the reflectivity properties of graphene in Ref. [20] using the polarization tensor was limited

to the case of sufficiently high frequencies, where one can omit the temperature-dependent part of this tensor.

The present paper develops complete quantum field theoretical description for the reflectivity of graphene over the entire range of real frequencies from zero to infinity. For this purpose we derive another representation for the polarization tensor of graphene in (2+1)-dimensional space-time which is valid not only at the imaginary Matsubara frequencies, but over the whole complex plane, specifically, along the real frequency axis. Since the beginning of 1960s it is known which representation of the polarization tensor allows for the correct analytic continuation [21]. Here we follow methods suggested in Refs. [21, 22]. In so doing, we compare our representation with that obtained in Ref. [10] and demonstrate quite a different behavior everywhere with exception of only the pure imaginary Matsubara frequencies. Furthermore, we consider the scattering frequency interval and find analytic asymptotic expressions for the polarization tensor and for both TM and TE reflectivities of graphene. The cases of low and high frequencies of incident electromagnetic waves with respect to the temperature are investigated. We also perform numerical computations of reflectivities and find the application regions of our asymptotic expressions. Finally, we compare quantum field theoretical results of this paper with those obtained previously [7, 8] using the local model for the conductivity of graphene. A good agreement is demonstrated for the TM reflectivities at both high and low frequencies. At the same time, the TE reflectivity is shown to depend on the angle of incidence on the contrary to a qualitative conclusion made previously [8].

The paper is organized as follows. In Sec. II we derive the polarization tensor for graphene applicable over the entire plane of complex frequency. Section III is devoted to the comparison with previously obtained expressions for the polarization tensor. The analytic asymptotic expressions for the polarization tensor and for both TM and TE reflectivities of graphene at high frequencies are obtained in Sec. IV. In Sec. V the same is done at low frequencies and the comparison with the results of numerical computations is presented. Section VI contains our conclusions and discussion. The Appendix contains details of derivation of the polarization tensor in Sec. II.

Throughout the paper we use units in which $\hbar = c = k_B = 1$, where k_B is the Boltzmann constant. The fundamental constants are restored for better understanding where necessary.

II. THE POLARIZATION TENSOR FOR GRAPHENE AT NONZERO TEMPERATURE

According to the Dirac model, the interaction of the electromagnetic field with the long wavelength (low frequency) electronic excitations in graphene can be described by relativistic quantum electrodynamics in (2+1)-dimensions, where the speed of light inside the graphene sheet is replaced with the Fermi velocity $v_F \approx 1/300$ [1, 2]. In this formalism, the Dirac equation is

$$(i\rlap{\not{D}} - e\rlap{\not{A}} - m)\psi = 0, \quad (1)$$

where m is the mass-gap parameter, A_μ is the vector-potential of the electromagnetic field,

$$\rlap{\not{D}} = \tilde{\gamma}^\mu \frac{\partial}{\partial x^\mu}, \quad \rlap{\not{A}} = \tilde{\gamma}^\mu A_\mu, \quad \tilde{\gamma}^\mu = \eta^\mu_\nu \gamma^\nu, \quad (2)$$

the Greek indices $\mu, \nu = 0, 1, 2$, γ^μ are the standard γ -matrices and the metric tensor η^μ_ν is given by

$$\eta^\mu_\nu = \text{diag}(1, v_F, v_F). \quad (3)$$

Note that we assume graphene situated at the plane (x^1, x^2) .

The polarization tensor for graphene at zero temperature was obtained in Ref. [9]. In Ref. [10] it was found at any nonzero temperature at all Matsubara frequencies using the Feynman parameter for a massive fermionic field and earlier, in the same representation, in Ref. [23] for a massless field, but with chemical potential. Here, we obtain another representation for the polarization tensor of graphene which is valid over the whole plane of complex frequencies including the real and imaginary frequency axes.

We start from the definition for the polarization tensor of graphene in the one-loop approximation in momentum representation [10, 24]

$$\begin{aligned} \Pi^{\mu\nu}(k) &= \Pi^{\mu\nu}(k_0, \mathbf{k}_\perp) \\ &= 8\pi i\alpha \int \frac{dq_0 d\mathbf{q}}{(2\pi)^3} \text{tr} \frac{1}{i\rlap{\not{q}} - m} \tilde{\gamma}^\mu \frac{1}{i\rlap{\not{q}} - i\rlap{\not{k}} - m} \tilde{\gamma}^\nu. \end{aligned} \quad (4)$$

Here, $k \equiv k^\mu = (k_0, \mathbf{k}_\perp) \equiv (\omega, \mathbf{k}_\perp)$ is the 3-momentum of an external photon, $k_0 = \omega$ is the frequency, $\mathbf{k}_\perp = (k^1, k^2)$, and $\alpha = e^2 \approx 1/137$ is the fine structure constant. In a similar way, the 3-momentum of a loop electronic excitation is $q \equiv q^\mu = (q_0, \mathbf{q}_\perp)$, $\mathbf{q}_\perp = (q^1, q^2)$ and we use the notations $\rlap{\not{q}} = \tilde{\gamma}^\mu q_\mu$, $\rlap{\not{k}} = \tilde{\gamma}^\mu k_\mu$. Note that for the purpose of calculating the

polarization tensor, the use of the standard 4×4 γ -matrices instead of 2×2 σ -matrices and an additional multiple 2 included in front of the right-hand side of Eq. (4) take into account $N = 4$ number of fermion species for graphene.

We are interested to find the polarization tensor of graphene at any temperature T . In order to introduce temperature within the Matsubara formalism, one should replace the integration over q_0 in Eq. (4) with the summation over the imaginary fermionic Matsubara frequencies

$$q_{0n} \equiv iq_{4n} = 2\pi i \left(n + \frac{1}{2} \right) T, \quad (5)$$

where $n = 0, \pm 1, \pm 2, \dots$. This replacement has the form

$$\int_{-\infty}^{\infty} \frac{dq_0}{2\pi} \rightarrow iT \sum_{n=-\infty}^{\infty}. \quad (6)$$

One should also replace the frequency $k_0 = \omega$ in the argument of $\Pi^{\mu\nu}$ in Eq. (4) with the imaginary bosonic Matsubara frequencies

$$k_{0l} = \omega_l \equiv ik_{4l} \equiv i\xi_l = 2\pi ilT, \quad (7)$$

where l is an integer number. Later it will be possible to turn the imaginary frequency back to real frequency.

At both zero and nonzero temperature (as well as at nonzero chemical potential μ), the polarization tensor is transversal, i.e., it holds

$$k_\mu \Pi^{\mu\nu}(k_0, \mathbf{k}_\perp) = 0. \quad (8)$$

Another useful property is that in the presence of graphene all components of the polarization tensor can be expressed in terms of two independent quantities with corresponding form factors [10]. Following Ref. [10], we use the 00-component and the trace of the polarization tensor

$$\Pi_{00}(\omega, \mathbf{k}_\perp), \quad \Pi_{\text{tr}}(\omega, \mathbf{k}_\perp) = \Pi_\mu^\mu(k_0, \mathbf{k}_\perp), \quad (9)$$

as independent quantities in further calculations. It is only in the special case $T = 0$ (here and below we put $\mu = 0$) that the quantities (9) are connected by the equation

$$\Pi_{\text{tr}}(\omega, \mathbf{k}_\perp) = -\frac{2\omega^2 - k_\perp^2(1 + v_F^2)}{k_\perp^2} \Pi_{00}(\omega, \mathbf{k}_\perp), \quad (10)$$

where $k_\perp = |\mathbf{k}_\perp|$. As shown below, the components (9) of the polarization tensor depend not on \mathbf{k}_\perp but on k_\perp .

Using the Maxwell equations describing an electromagnetic field outside the surface of graphene and the standard matching conditions it is possible to express the reflection coefficients on graphene for both independent polarizations via the polarization tensor. The result is [10]:

$$\begin{aligned} r_{\text{TM}}(\omega, k_{\perp}) &= \frac{1}{1 + Q_{\text{TM}}^{-1}(\omega, k_{\perp})}, \\ r_{\text{TE}}(\omega, k_{\perp}) &= -\frac{1}{1 + Q_{\text{TE}}^{-1}(\omega, k_{\perp})}, \end{aligned} \quad (11)$$

where the quantities $Q_{\text{TM(TE)}}$ are given by

$$\begin{aligned} Q_{\text{TM}}(\omega, k_{\perp}) &= \frac{p(\omega, k_{\perp})}{2ik_{\perp}^2} \Pi_{00}(\omega, k_{\perp}), \\ Q_{\text{TE}}(\omega, k_{\perp}) &= -\frac{1}{2ip(\omega, k_{\perp})} \Pi_{\text{tr}}(\omega, k_{\perp}) - \frac{p(\omega, k_{\perp})}{2ik_{\perp}^2} \Pi_{00}(\omega, k_{\perp}). \end{aligned} \quad (12)$$

Here, we have introduced the notation

$$p(\omega, k_{\perp}) = \sqrt{\omega^2 - k_{\perp}^2}. \quad (13)$$

Substituting Eq. (12) in Eq. (11), one obtains the reflection coefficients in terms of the polarization tensor [10],

$$\begin{aligned} r_{\text{TM}}(\omega, k_{\perp}) &= \frac{p(\omega, k_{\perp})\Pi_{00}}{2ik_{\perp}^2 + p(\omega, k_{\perp})\Pi_{00}}, \\ r_{\text{TE}}(\omega, k_{\perp}) &= -\frac{k_{\perp}^2 \Pi_{\text{tr}} + p^2(\omega, k_{\perp})\Pi_{00}}{-2ik_{\perp}^2 p(\omega, k_{\perp}) + k_{\perp}^2 \Pi_{\text{tr}} + p^2(\omega, k_{\perp})\Pi_{00}}, \end{aligned} \quad (14)$$

where, for the sake of brevity, we put $\Pi_{00(\text{tr})} \equiv \Pi_{00(\text{tr})}(\omega, k_{\perp})$.

Equations (12) and (14) define the reflection coefficients (11) in the Minkowskian region, i.e., for real ω and $\omega \geq k_{\perp}$ such that the quantity $p(\omega, k_{\perp})$ defined in Eq. (13) (it has an interpretation of the wave vector component perpendicular to the graphene sheet) is also real. The transition to the Euclidean region is done by putting $\omega = i\xi$. Then Eq. (12) turns into

$$\begin{aligned} Q_{\text{TM}}(i\xi, k_{\perp}) &= \frac{q(\xi, k_{\perp})}{2k_{\perp}^2} \Pi_{00}(i\xi, k_{\perp}), \\ Q_{\text{TE}}(i\xi, k_{\perp}) &= \frac{1}{2q(\xi, k_{\perp})} \Pi_{\text{tr}}(i\xi, k_{\perp}) - \frac{q(\xi, k_{\perp})}{2k_{\perp}^2} \Pi_{00}(i\xi, k_{\perp}), \end{aligned} \quad (15)$$

where

$$q(\xi, k_{\perp}) = \sqrt{\xi^2 + k_{\perp}^2} = -ip(i\xi, k_{\perp}). \quad (16)$$

Substituting Eq. (15) in Eq. (11) taken at $\omega = i\xi$, one obtains

$$\begin{aligned} r_{\text{TM}}(i\xi, k_{\perp}) &= \frac{q(\xi, k_{\perp})\Pi_{00}}{2k_{\perp}^2 + q(\xi, k_{\perp})\Pi_{00}}, \\ r_{\text{TE}}(i\xi, k_{\perp}) &= -\frac{k_{\perp}^2\Pi_{\text{tr}} - q^2(\xi, k_{\perp})\Pi_{00}}{2q(\xi, k_{\perp})k_{\perp}^2 + k_{\perp}^2\Pi_{\text{tr}} - q^2(\xi, k_{\perp})\Pi_{00}}, \end{aligned} \quad (17)$$

where $\Pi_{00(\text{tr})} \equiv \Pi_{00(\text{tr})}(i\xi, k_{\perp})$.

We are coming now to the calculation of polarization tensor of graphene at any temperature T . It is convenient to represent the independent quantities (9) considered at the imaginary Matsubara frequencies in the form

$$\Pi_{00(\text{tr})}(i\xi_l, \mathbf{k}_{\perp}) = \Pi_{00(\text{tr})}^{(0)}(i\xi_l, \mathbf{k}_{\perp}) + \Delta_T \Pi_{00(\text{tr})}(i\xi_l, \mathbf{k}_{\perp}), \quad (18)$$

where $\Pi_{00(\text{tr})}^{(0)}(i\xi_l, \mathbf{k}_{\perp})$ is the 00-component (trace) of the polarization tensor at $T = 0$ but calculated at the imaginary bosonic Matsubara frequencies $ik_{4l} = i\xi_l$, and $\Delta_T \Pi_{00(\text{tr})}(i\xi_l, k_{\perp})$ is the thermal correction which explicitly depends on the temperature and goes to zero in the limiting case $T \rightarrow 0$. The explicit expressions for $\Pi_{00(\text{tr})}^{(0)}$ are well known [9]

$$\begin{aligned} \Pi_{00}^{(0)}(i\xi_l, k_{\perp}) &= \frac{\alpha k_{\perp}^2}{\tilde{q}^2(\xi_l, k_{\perp})} \Phi(\xi_l, k_{\perp}), \\ \Pi_{\text{tr}}^{(0)}(i\xi_l, k_{\perp}) &= \alpha \frac{q^2(\xi_l, k_{\perp}) + \tilde{q}^2(\xi_l, k_{\perp})}{\tilde{q}^2(\xi_l, k_{\perp})} \Phi(\xi_l, k_{\perp}), \end{aligned} \quad (19)$$

where

$$\begin{aligned} \tilde{q}(\xi_l, k_{\perp}) &= \sqrt{\xi_l^2 + v_{\text{F}}^2 k_{\perp}^2}, \\ \Phi(\xi_l, k_{\perp}) &= 4 \left[m + \frac{\tilde{q}^2(\xi_l, k_{\perp}) - 4m^2}{2\tilde{q}(\xi_l, k_{\perp})} \arctan \frac{\tilde{q}(\xi_l, k_{\perp})}{2m} \right]. \end{aligned} \quad (20)$$

The expressions for $\Delta_T \Pi_{00(\text{tr})}$ valid at the imaginary Matsubara frequencies were obtained in Ref. [10]. Here, we derive the representation for $\Delta_T \Pi_{00(\text{tr})}$ which admits the analytic continuation to the real frequency axis (see Appendix A). According to Eqs. (A18)–(A21) the result is

$$\begin{aligned} \Delta_T \Pi_{00(\text{tr})}(i\xi_l, k_{\perp}) &= \frac{16\alpha}{v_{\text{F}}^2} \int_0^{\infty} dq_{\perp} \frac{q_{\perp}}{\Gamma(q_{\perp})} \frac{1}{e^{\Gamma(q_{\perp})/T} + 1} \\ &\times \left[1 + \frac{1}{2} \sum_{\lambda=\pm 1} \frac{M_{00(\text{tr})}(\xi_l, k_{\perp}, q_{\perp})}{N(\xi_l, k_{\perp}, q_{\perp})} \right], \end{aligned} \quad (21)$$

where $q_\perp = |\mathbf{q}_\perp|$ and the following notations are introduced:

$$\begin{aligned}
N(\xi_l, k_\perp, q_\perp) &= [Q^2(\xi_l, k_\perp, q_\perp) - (2v_F k_\perp q_\perp)^2]^{1/2}, \\
Q(\xi_l, k_\perp, q_\perp) &= \tilde{q}^2(\xi_l, k_\perp) - 2i\lambda\xi_l\Gamma(q_\perp), \\
\Gamma(q_\perp) &= \sqrt{q_\perp^2 + m^2}, \\
M_{00}(\xi_l, k_\perp, q_\perp) &= 4\Gamma^2(q_\perp) - \tilde{q}^2(\xi_l, k_\perp) + 4i\lambda\xi_l\Gamma(q_\perp), \\
M_{\text{tr}}(\xi_l, k_\perp, q_\perp) &= -\tilde{q}^2(\xi_l, k_\perp) + 4v_F^2 m^2 \\
&\quad + 4(1 - v_F^2) [\Gamma^2(q_\perp) + i\lambda\xi_l\Gamma(q_\perp)].
\end{aligned} \tag{22}$$

Note that for all $\xi > 0$ including the Matsubara frequencies ξ_l with $l \geq 1$ the summation in $\lambda = \pm 1$ in Eq. (21) can be equivalently represented as

$$\frac{1}{2} \sum_{\lambda=\pm 1} \frac{M_{00(\text{tr})}}{N} = \text{Re} \frac{M_{00(\text{tr})}}{N}. \tag{23}$$

We emphasize that in order to obtain the correct result in Eq. (21) at $\xi_0 = 0$, one should first make the summation in $\lambda = \pm 1$ at $\xi > 0$ and then consider the limit $\xi \rightarrow 0$. Note that if one puts $\xi_0 = 0$ first, the subsequent summation in $\lambda = \pm 1$ would lead to a complex result for some relationships between k_\perp and q_\perp in contradiction with the fact that the polarization tensor along the imaginary frequency axis must be real. The proposed continuation of the expression (21) to zero Matsubara frequency is equivalent to the use of Eq. (23) at all $\xi \geq 0$. It is also confirmed in Sec. III by the comparison with another representation for the polarization tensor of graphene.

In the massless case, $m = 0$, the above representation for the polarization tensor of graphene can be simplified. Using Eqs. (19) and (20), for the zero temperature parts one obtains

$$\begin{aligned}
\Pi_{00}^{(0)}(i\xi_l, k_\perp) &= \frac{\pi\alpha k_\perp^2}{\tilde{q}(\xi_l, k_\perp)}, \\
\Pi_{\text{tr}}^{(0)}(i\xi_l, k_\perp) &= \pi\alpha \frac{q^2(\xi_l, k_\perp) + \tilde{q}^2(\xi_l, k_\perp)}{\tilde{q}(\xi_l, k_\perp)}.
\end{aligned} \tag{24}$$

For the thermal correction in the massless case $\Gamma(q_\perp) = q_\perp$ and from Eq. (22) we have

$$N(\xi_l, k_\perp, q_\perp) = \tilde{q}(\xi_l, k_\perp) W(\xi_l, k_\perp, q_\perp), \tag{25}$$

where

$$W(\xi_l, k_\perp, q_\perp) = [\tilde{q}^2(\xi_l, k_\perp) - 4i\lambda\xi_l q_\perp - 4q_\perp^2]^{1/2}. \tag{26}$$

In a similar way, from Eq. (22) in the massless case one arrives at

$$\begin{aligned} M_{00}(\xi_l, k_\perp, q_\perp) &= -W^2(\xi_l, k_\perp, q_\perp), \\ M_{\text{tr}}(\xi_l, k_\perp, q_\perp) &= -(1 - v_F^2)W^2(\xi_l, k_\perp, q_\perp) - v_F^2 \tilde{q}^2(\xi_l, k_\perp). \end{aligned} \quad (27)$$

Substituting Eqs. (25) and (27) in Eq. (21), we find the thermal correction to the polarization tensor in the massless case

$$\begin{aligned} \Delta_T \Pi_{00}(i\xi_l, k_\perp) &= \frac{16\alpha}{v_F^2} \int_0^\infty dq_\perp \frac{1}{e^{q_\perp/T} + 1} \\ &\times \left[1 - \frac{1}{2} \sum_{\lambda=\pm 1} \frac{W(\xi_l, k_\perp, q_\perp)}{\tilde{q}(\xi_l, k_\perp)} \right], \\ \Delta_T \Pi_{\text{tr}}(i\xi_l, k_\perp) &= \frac{16\alpha}{v_F^2} \int_0^\infty dq_\perp \frac{1}{e^{q_\perp/T} + 1} \\ &\times \left\{ 1 - \frac{1}{2} \sum_{\lambda=\pm 1} \left[(1 - v_F^2) \frac{W(\xi_l, k_\perp, q_\perp)}{\tilde{q}(\xi_l, k_\perp)} + v_F^2 \frac{\tilde{q}(\xi_l, k_\perp)}{W(\xi_l, k_\perp, q_\perp)} \right] \right\}. \end{aligned} \quad (28)$$

Finally, we consider the Minkowskian region by turning the imaginary frequency to the real frequency axis in accordance to $\omega = i\xi$. Here we have several frequency subintervals. For the lowest frequencies, $\omega \leq v_F k_\perp$, all the above formulas hold literally and \tilde{q} remains real after putting $\xi^2 = -\omega^2$. The interval where surface plasmons may exist goes next. It is characterized by

$$\begin{aligned} v_F k_\perp &< \omega < k_\perp, \\ q(\omega, k_\perp) &= \sqrt{-\omega^2 + k_\perp^2}, \quad \tilde{p}(\omega, k_\perp) = \sqrt{\omega^2 - v_F^2 k_\perp^2}, \end{aligned} \quad (29)$$

where q and \tilde{p} are real. The scattering interval

$$k_\perp \leq \omega \quad (30)$$

is the most important one because it corresponds to real photons on a mass-shell. Here, both the quantity $p(\omega, k_\perp)$ defined in Eq. (13) and $\tilde{p}(\omega, k_\perp)$ defined in Eq. (29) are real.

In the plasmonic and in the scattering frequency intervals, the polarization tensor has a similar form. At zero temperature it is given by

$$\begin{aligned} \Pi_{00}^{(0)}(\omega, k_\perp) &= -\frac{\alpha k_\perp^2}{\tilde{p}^2(\omega, k_\perp)} \Phi(\omega, k_\perp), \\ \Pi_{\text{tr}}^{(0)}(\omega, k_\perp) &= \alpha \frac{p^2(\omega, k_\perp) + \tilde{p}^2(\omega, k_\perp)}{\tilde{p}^2(\omega, k_\perp)} \Phi(\omega, k_\perp), \end{aligned} \quad (31)$$

where the function Φ along the real frequency axis is defined as

$$\Phi(\omega, k_{\perp}) = \begin{cases} 4 \left[m - \frac{\tilde{p}^2(\omega, k_{\perp}) + 4m^2}{2\tilde{p}(\omega, k_{\perp})} \operatorname{arctanh} \frac{\tilde{p}(\omega, k_{\perp})}{2m} \right], & \omega \leq \sqrt{v_F^2 k_{\perp}^2 + 4m^2}, \\ 4 \left[m - \frac{\tilde{p}^2(\omega, k_{\perp}) + 4m^2}{2\tilde{p}(\omega, k_{\perp})} \left(\operatorname{arctanh} \frac{2m}{\tilde{p}(\omega, k_{\perp})} + \frac{i\pi}{2} \right) \right], & \omega > \sqrt{v_F^2 k_{\perp}^2 + 4m^2}. \end{cases} \quad (32)$$

The thermal correction to the polarization tensor in the plasmonic and scattering frequency intervals takes the form of Eq. (21),

$$\begin{aligned} \Delta_T \Pi_{00(\text{tr})}(\omega, k_{\perp}) &= \frac{16\alpha}{v_F^2} \int_0^{\infty} dq_{\perp} \frac{q_{\perp}}{\Gamma(q_{\perp})} \frac{1}{e^{\Gamma(q_{\perp})/T} + 1} \\ &\times \left[1 + \frac{1}{2} \sum_{\lambda=\pm 1} \frac{M_{00(\text{tr})}(\omega, k_{\perp}, q_{\perp})}{N(\omega, k_{\perp}, q_{\perp})} \right]. \end{aligned} \quad (33)$$

Here, the denominator N takes different forms depending on the value of the quantity [compare with Eq. (22)]

$$Q(\omega, k_{\perp}, q_{\perp}) = -\tilde{p}^2(\omega, k_{\perp}) - 2\lambda\omega\Gamma(q_{\perp}). \quad (34)$$

If $|Q(\omega, k_{\perp}, q_{\perp})| \geq 2v_F k_{\perp} q_{\perp}$ we have

$$\begin{aligned} N(\omega, k_{\perp}, q_{\perp}) &= \operatorname{sign} Q(\omega, k_{\perp}, q_{\perp}) \\ &\times [Q^2(\omega, k_{\perp}, q_{\perp}) - (2v_F k_{\perp} q_{\perp})^2]^{1/2}, \end{aligned} \quad (35)$$

whereas if $|Q(\omega, k_{\perp}, q_{\perp})| < 2v_F k_{\perp} q_{\perp}$

$$N(\omega, k_{\perp}, q_{\perp}) = -i [-Q^2(\omega, k_{\perp}, q_{\perp}) + (2v_F k_{\perp} q_{\perp})^2]^{1/2} \quad (36)$$

holds. Two other quantities entering Eq. (33) are given by

$$\begin{aligned} M_{00}(\omega, k_{\perp}, q_{\perp}) &= 4\Gamma^2(q_{\perp}) + \tilde{p}^2(\omega, k_{\perp}) + 4\lambda\omega\Gamma(q_{\perp}), \\ M_{\text{tr}}(\omega, k_{\perp}, q_{\perp}) &= \tilde{p}^2(\omega, k_{\perp}) + 4v_F^2 m^2 \\ &+ 4(1 - v_F^2) [\Gamma^2(q_{\perp}) + \lambda\omega\Gamma(q_{\perp})]. \end{aligned} \quad (37)$$

Note that in the plasmonic frequency interval the denominator N has no zeroes, but in the scattering interval with $\lambda = -1$ it has two zeros at

$$(q_{\perp})_{1,2} = \mp \frac{v_F k_{\perp}}{2} + \frac{\omega}{2} \sqrt{1 - \frac{4m^2}{\tilde{p}^2(\omega, k_{\perp})}}. \quad (38)$$

These zeros result in the integrable singularities.

Now we consider the massless case in the scattering interval where Eqs. (33) and (35)–(37) for the polarization tensor can be significantly simplified. At zero temperature the result follows from Eqs. (31) and (32) in the limiting case $m \rightarrow 0$ [20],

$$\begin{aligned}\Pi_{00}^{(0)}(\omega, k_\perp) &= \frac{i\pi\alpha k_\perp^2}{\tilde{p}(\omega, k_\perp)}, \\ \Pi_{\text{tr}}^{(0)}(\omega, k_\perp) &= -i\pi\alpha \frac{p^2(\omega, k_\perp) + \tilde{p}^2(\omega, k_\perp)}{\tilde{p}(\omega, k_\perp)}.\end{aligned}\tag{39}$$

For the thermal correction in the massless case from Eqs. (35) and (36) one obtains

$$N(\omega, k_\perp, q_\perp) = \tilde{p}(\omega, k_\perp)W(\omega, k_\perp, q_\perp),\tag{40}$$

where

$$W^2(\omega, k_\perp, q_\perp) = \tilde{p}^2(\omega, k_\perp) + 4\lambda\omega q_\perp + 4q_\perp^2.\tag{41}$$

The explicit expression for $W(\omega, k_\perp, q_\perp)$ follows from Eqs. (35) and (36). It is different for different $\lambda = \pm 1$ and depends on the value of q_\perp . Thus, for $\lambda = 1$ and for any q_\perp it holds

$$W(\omega, k_\perp, q_\perp) = -[\tilde{p}^2(\omega, k_\perp) + 4\omega q_\perp + 4q_\perp^2]^{1/2},\tag{42}$$

whereas for $\lambda = -1$ we have

$$W(\omega, k_\perp, q_\perp) = \begin{cases} -[\tilde{p}^2(\omega, k_\perp) - 4\omega q_\perp + 4q_\perp^2]^{1/2}, & 2q_\perp \leq \omega - v_F k_\perp, \\ -i[-\tilde{p}^2(\omega, k_\perp) + 4\omega q_\perp - 4q_\perp^2]^{1/2}, & \omega - v_F k_\perp < 2q_\perp < \omega + v_F k_\perp, \\ [\tilde{p}^2(\omega, k_\perp) - 4\omega q_\perp + 4q_\perp^2]^{1/2}, & 2q_\perp \geq \omega + v_F k_\perp. \end{cases}\tag{43}$$

In so doing all expressions under the square roots in Eqs. (42) and (43) are positive.

Using Eq. (41), the quantities M_{00} and M_{tr} defined in Eq. (37) can be written in the massless case as

$$\begin{aligned}M_{00}(\omega, k_\perp, q_\perp) &= W^2(\omega, k_\perp, q_\perp), \\ M_{\text{tr}}(\omega, k_\perp, q_\perp) &= (1 - v_F^2)W^2(\omega, k_\perp, q_\perp) + v_F^2\tilde{p}^2(\omega, k_\perp).\end{aligned}\tag{44}$$

Substituting Eqs. (40) and (44) in Eq. (33), we arrive at the thermal correction to the

polarization tensor of graphene with $m = 0$ in the scattering interval,

$$\begin{aligned}
\Delta_T \Pi_{00}(\omega, k_\perp) &= \frac{16\alpha}{v_F^2} \int_0^\infty dq_\perp \frac{1}{e^{q_\perp/T} + 1} \\
&\times \left[1 + \frac{1}{2} \sum_{\lambda=\pm 1} \frac{W(\omega, k_\perp, q_\perp)}{\tilde{p}(\omega, k_\perp)} \right], \\
\Delta_T \Pi_{\text{tr}}(\omega, k_\perp) &= \frac{16\alpha}{v_F^2} \int_0^\infty dq_\perp \frac{1}{e^{q_\perp/T} + 1} \\
&\times \left\{ 1 + \frac{1}{2} \sum_{\lambda=\pm 1} \left[(1 - v_F^2) \frac{W(\omega, k_\perp, q_\perp)}{\tilde{p}(\omega, k_\perp)} + v_F^2 \frac{\tilde{p}(\omega, k_\perp)}{W(\omega, k_\perp, q_\perp)} \right] \right\}.
\end{aligned} \tag{45}$$

Note also that in the scattering interval (40) under consideration here, the denominator of $\Delta_T \Pi_{\text{tr}}$ has zeros at

$$(q_\perp)_{1,2} = \frac{\omega \pm v_F k_\perp}{2}. \tag{46}$$

These singularities are integrable.

III. COMPARISON BETWEEN DIFFERENT REPRESENTATIONS FOR THE POLARIZATION TENSOR OF GRAPHENE

In previous section, we have obtained the polarization tensor of graphene at the imaginary Matsubara frequencies $i\xi_l$ and found its analytic continuation to the whole plane of complex frequencies including the real frequency axis. As discussed in Sec. I, another representation for the polarization tensor is contained in Ref. [10]. Here we compare both representations and demonstrate that the tensor of Ref. [10] can be used solely at the Matsubara frequencies, but not along the real frequency axis [i.e., Eqs. (13) and (24) in Ref. [10]]. For the sake of brevity, here we restrict ourselves to the case of gapless graphene ($m = 0$), which is used in our calculations of reflectivities in the following sections.

First of all we note that the polarization tensor of graphene at zero temperature calculated at the imaginary Matsubara frequencies is given by Eq. (24) in both representations. Because of this, the subjects of our comparison are only the thermal corrections $\Delta_T \Pi_{00(\text{tr})}$. Taking into account the structure of the reflection coefficients (17), below we compare different representations not for $\Delta_T \Pi_{00}(i\xi_l, k_\perp)$ and $\Delta_T \Pi_{\text{tr}}(i\xi_l, k_\perp)$ but for $\Delta_T \Pi_{00}(i\xi_l, k_\perp)$ and the following quantity:

$$\Delta_T \Pi(i\xi_l, k_\perp) \equiv k_\perp^2 \Delta_T \Pi_{\text{tr}}(i\xi_l, k_\perp) - q^2(\xi_l, k_\perp) \Delta_T \Pi_{00}(i\xi_l, k_\perp). \tag{47}$$

In our representation $\Delta_T \Pi_{00}(i\xi_l, k_\perp)$ is given by the first line of Eq. (28) and the explicit expression for $\Delta_T \Pi(i\xi_l, k_\perp)$ follows from Eq. (28):

$$\Delta_T \Pi(i\xi_l, k_\perp) = \frac{16\alpha}{v_F^2} \int_0^\infty \frac{dq_\perp}{e^{q_\perp/T} + 1} \left[-\xi_l^2 + \tilde{q}^2(\xi_l, k_\perp) \operatorname{Re} \frac{W(\xi_l, k_\perp, q_\perp)}{\tilde{q}(\xi_l, k_\perp)} - v_F^2 k_\perp^2 \operatorname{Re} \frac{\tilde{q}(\xi_l, k_\perp)}{W(\xi_l, k_\perp, q_\perp)} \right]. \quad (48)$$

We also take into account Eq. (23). Our representation should be compared with the following alternative results of Ref. [10] (see also Ref. [14]) which we notate by an upper index (a):

$$\begin{aligned} \Delta_T \Pi_{00}^{(a)}(i\xi_l, k_\perp) &= \frac{8\alpha}{v_F^2} \int_0^1 dx \left\{ T \ln [1 + 2 \cos(\xi_l x/T) e^{-\Theta_T(x, \xi_l, k_\perp)} + e^{-2\Theta_T(x, \xi_l, k_\perp)}] - \frac{\xi_l}{2} (1 - 2x) \frac{\sin(\xi_l x/T)}{\cosh \Theta_T(x, \xi_l, k_\perp) + \cos(\xi_l x/T)} \right. \\ &\quad \left. + \frac{\xi_l^2 \sqrt{x(1-x)}}{\tilde{q}(\xi_l, k_\perp)} \frac{\cos(\xi_l x/T) + e^{-\Theta_T(x, \xi_l, k_\perp)}}{\cosh \Theta_T(x, \xi_l, k_\perp) + \cos(\xi_l x/T)} \right\}, \\ \Delta_T \Pi^{(a)}(i\xi_l, k_\perp) &= -\frac{8\alpha}{v_F^2} \int_0^1 dx \left\{ T \xi_l^2 \ln [1 + 2 \cos(\xi_l x/T) e^{-\Theta_T(x, \xi_l, k_\perp)} + e^{-2\Theta_T(x, \xi_l, k_\perp)}] - [2\tilde{q}^2(\xi_l, k_\perp) - \xi_l^2] \frac{\xi_l}{2} (1 - 2x) \frac{\sin(\xi_l x/T)}{\cosh \Theta_T(x, \xi_l, k_\perp) + \cos(\xi_l x/T)} \right. \\ &\quad \left. + \sqrt{x(1-x)} \tilde{q}^3(\xi_l, k_\perp) \frac{\cos(\xi_l x/T) + e^{-\Theta_T(x, \xi_l, k_\perp)}}{\cosh \Theta_T(x, \xi_l, k_\perp) + \cos(\xi_l x/T)} \right\}, \end{aligned} \quad (49)$$

where

$$\Theta_T(x, \xi_l, k_\perp) = \frac{\tilde{q}(\xi_l, k_\perp)}{T} \sqrt{x(1-x)}. \quad (50)$$

As shown in Refs. [10–12], for graphene the major contribution to the thermal correction comes from the zero Matsubara frequency. We start from this case and by putting $l = 0$, $\xi_0 = 0$ in Eqs. (28) and (48) obtain

$$\begin{aligned} \Delta_T \Pi_{00}(0, k_\perp) &= \frac{16\alpha}{v_F^2} \left(\int_0^\infty \frac{dq_\perp}{e^{q_\perp/T} + 1} - \frac{1}{v_F k_\perp} \int_0^{v_F k_\perp/2} dq_\perp \frac{\sqrt{v_F^2 k_\perp^2 - 4q_\perp^2}}{e^{q_\perp/T} + 1} \right), \\ \Delta_T \Pi(0, k_\perp) &= 16\alpha \int_0^{v_F k_\perp/2} \frac{dq_\perp}{e^{q_\perp/T} + 1} \left(-\frac{v_F k_\perp^3}{\sqrt{v_F^2 k_\perp^2 - 4q_\perp^2}} + \frac{k_\perp}{v_F} \sqrt{v_F^2 k_\perp^2 - 4q_\perp^2} \right). \end{aligned} \quad (51)$$

By introducing the new variable $z = 2q_\perp/(v_F k_\perp)$, these results can be rewritten in the form

$$\begin{aligned} \Delta_T \Pi_{00}(0, k_\perp) &= \frac{16\alpha}{v_F^2} \left(T \ln 2 - \frac{v_F k_\perp}{2} \int_0^1 dz \frac{\sqrt{1-z^2}}{e^{Az/2} + 1} \right), \\ \Delta_T \Pi(0, k_\perp) &= -8\alpha v_F k_\perp^3 \int_0^1 \frac{dz}{e^{Az/2} + 1} \frac{z^2}{\sqrt{1-z^2}}, \end{aligned} \quad (52)$$

where $A \equiv v_F k_\perp / T$.

The alternative expressions of Ref. [10] are obtained by putting $l = 0$, $\xi_0 = 0$ in Eq. (49)

$$\begin{aligned}\Delta_T \Pi_{00}^{(a)}(0, k_\perp) &= \frac{8\alpha T}{v_F^2} \int_0^1 dx \ln \left[1 + 2e^{-A\sqrt{x(1-x)}} + e^{-2A\sqrt{x(1-x)}} \right], \\ \Delta_T \Pi^{(a)}(0, k_\perp) &= -8\alpha v_F k_\perp^3 \int_0^1 dx \sqrt{x(1-x)} \frac{1 + e^{-A\sqrt{x(1-x)}}}{\cosh[A\sqrt{x(1-x)}] + 1}.\end{aligned}\quad (53)$$

By making transformations in the first line of Eq. (53) and integrating by parts, we have

$$\begin{aligned}\Delta_T \Pi_{00}^{(a)}(0, k_\perp) &= \frac{16\alpha T}{v_F^2} \int_0^1 dx \ln \left[1 + e^{-A\sqrt{x(1-x)}} \right] \\ &= \frac{16\alpha T}{v_F^2} \left[T \ln 2 + v_F k_\perp \int_0^{1/2} dx \frac{x(1-2x)}{2\sqrt{x(1-x)}} \frac{1}{e^{A\sqrt{x(1-x)}} + 1} \right. \\ &\quad \left. + v_F k_\perp \int_{1/2}^1 dx \frac{x(1-2x)}{2\sqrt{x(1-x)}} \frac{1}{e^{A\sqrt{x(1-x)}} + 1} \right].\end{aligned}\quad (54)$$

In both these integrals we introduce the new variable

$$\begin{aligned}y &= 2\sqrt{x(1-x)}, & dy &= \frac{1-2x}{\sqrt{x(1-x)}}, \\ x_{1,2} &= \frac{1 \pm \sqrt{1-y^2}}{2},\end{aligned}\quad (55)$$

where the signs plus and minus correspond to the second and first integrals, respectively.

This leads to the result coinciding with the first line of Eq. (52).

In a similar way, the second line of Eq. (53) can be represented in the form

$$\begin{aligned}\Delta_T \Pi^{(a)}(0, k_\perp) &= -16\alpha v_F k_\perp^3 \int_0^1 dx \frac{\sqrt{x(1-x)}}{e^{A\sqrt{x(1-x)}} + 1} \\ &= -16\alpha v_F k_\perp^3 \left[\int_0^{1/2} dx \frac{\sqrt{x(1-x)}}{e^{A\sqrt{x(1-x)}} + 1} + \int_{1/2}^1 dx \frac{\sqrt{x(1-x)}}{e^{A\sqrt{x(1-x)}} + 1} \right].\end{aligned}\quad (56)$$

After introducing the new variable (55), where the sign plus corresponds to the second integral and the sign minus to the first, Eq. (56) coincides with the second line in Eq. (52).

Thus, it holds

$$\Delta_T \Pi_{00}(0, k_\perp) = \Delta_T \Pi_{00}^{(a)}(0, k_\perp) \quad \Delta_T \Pi(0, k_\perp) = \Delta_T \Pi^{(a)}(0, k_\perp). \quad (57)$$

In fact our representation for the polarization tensor in Eqs. (28) and (48) coincides with that of Ref. [10] [see Eq. (49)] not only at zeroth but at all Matsubara frequencies. To

illustrate this, in the second column of Table I we present the values of $\Delta_T \Pi_{00}^{(a)}$, normalized by the coefficient $C \equiv 16\alpha T/v_F^2$, which are computed using the first formula of Eq. (49) at $k_\perp = 10\xi_1$ and first eleven nonzero Matsubara frequencies indicated in the first column. In the third column of this table, our results for $\Delta_T \Pi_{00}$ computed using the first formula of Eq. (28) are presented. As can be seen in Table I, both sets of results coincide up to a high accuracy. The fourth column contains the relative thermal correction $\Delta_T \Pi_{00}/\Pi_{00}^{(0)}$, which decreases quickly with increasing l . Similar computations were performed at $k_\perp = 0.5\xi_1$, $100\xi_1$ and $500\xi_1$. It was found that in all cases the values of $\Delta_T \Pi_{00}(i\xi_l, k_\perp)$ computed using different representations coincide. Note that with respect to the Casimir effect [25, 26] the value $k_\perp = 10\xi_1$ is the magnitude of the wave vector giving the major contribution to the force between two parallel graphene sheets spaced at the separation distance 100 nm.

In Table II similar computational results for the quantities $\Delta_T \Pi(i\xi_l, k_\perp)$ and $\Delta_T \Pi^{(a)}(i\xi_l, k_\perp)$ are presented normalized by the coefficient $D \equiv 8\alpha\xi_1^3/v_F^2$. As can be seen in this table, the thermal correction $\Delta_T \Pi$ computed using the representation of Ref. [10] [i.e., the second formula of Eq. (49), column 2] and the approach of this paper, i.e., Eq. (48) (column 3) coincide at all Matsubara frequencies (column 1). The same values of k_\perp , as in Table I, were used in computations. The relative thermal correction is given in column 4. Thus, one can conclude that

$$\Delta_T \Pi_{00}(i\xi_l, k_\perp) = \Delta_T \Pi_{00}^{(a)}(i\xi_l, k_\perp) \quad \Delta_T \Pi(i\xi_l, k_\perp) = \Delta_T \Pi^{(a)}(i\xi_l, k_\perp). \quad (58)$$

It can be easily seen, however, that the polarization tensors of graphene obtained in Ref. [10] and in this paper behave quite differently at all frequencies other than the Matsubara frequencies. To see this, in Fig. 1 we plot $10^5 \times \Delta_T \Pi_{00}/C$ (a) and $\Delta_T \Pi_{00}^{(a)}/C$ (b) as functions of ξ/ξ_1 at $k_\perp = 10\xi_1$. In so doing, the quantities $\Delta_T \Pi_{00}$ and $\Delta_T \Pi_{00}^{(a)}$ were computed using the first formulas of Eqs. (28) and (49), respectively, where the Matsubara frequencies ξ_l are replaced with the continuous frequency ξ [see Eqs. (32) and (33) of Ref. [27] where the polarization tensor of Ref. [10] is written along continuous pure imaginary frequencies]. As is seen in Fig. 1(a,b), our thermal correction decreases monotonously with increasing ξ , whereas the thermal correction of Ref. [10] oscillates between the values it takes at the Matsubara frequencies. This is a nonphysical analytic continuation from the set of Matsubara frequencies to the imaginary frequency axis and, as a consequence, to the whole plane of complex frequencies including the real frequency axis (see Sec. IV for the physical results).

In Fig. 2(a,b) we present the respective results for the quantity $\Delta_T\Pi(i\xi, k_\perp)$ at $k_\perp = 10\xi_1$. Computations were performed in the framework of our formalism by Eq. (48) [Fig. 2(a)] and using the formalism of Ref. [10] by the second formula of Eq. (49) [Fig. 2(b)]. The quantities $10^4 \times \Delta_T\Pi/D$ and $\Delta_T\Pi^{(a)}/D$ are again plotted as functions of continuous frequency along the imaginary frequency axis. In our formalism, dependence of the thermal correction $\Delta_T\Pi$ on the frequency is again monotonous, whereas the quantity $\Delta_T\Pi^{(a)}$ oscillates taking the same values as $\Delta_T\Pi$ only at the Matsubara frequencies. The respective continuation of $\Delta_T\Pi^{(a)}$ to the real frequency axis does not possess necessary physical properties (see Sec. IV). This is an example of the well known general situation in the complex analysis that a sequence $f(l)$ with no accumulation point can give rise to different analytic functions $F(z)$ such that $F(l) = f(l)$. For example, the function $\Gamma(z+1)$ provides an analytic continuation of $n!$ to the entire complex plane, but this continuation is not unique. In particular, the analytic function, e. g., of the form $\Gamma(z+1) + C \sin(\pi z)$, where $C = \text{const}$, also provides the desired continuation.

IV. REFLECTIVITY OF GRAPHENE AT HIGH FREQUENCIES

Here, we find analytic asymptotic expressions for the polarization tensor of graphene in the scattering frequency interval (30) and respective graphene reflectivities at high frequencies satisfying the condition $\omega \gg T$. If we restore the fundamental constants, this condition takes the form

$$\omega \gg \omega_T \equiv \frac{k_B T}{\hbar}, \quad (59)$$

where ω_T is so called thermal frequency. For example, at room temperature $T = 300$ K the thermal frequency $\omega_T \approx 3.9 \times 10^{13}$ rad/s, i.e., Eq. (59) is well applicable in the optical range and at all higher frequencies.

Calculations are done starting from Eq. (45) for $\Delta_T\Pi_{00}(\omega, k_\perp)$ along the real frequency axis and the following expression for $\Delta_T\Pi(\omega, k_\perp)$, entering the reflection coefficient r_{TE} in

Eq. (14), which is obtained from Eq. (45):

$$\begin{aligned}\Delta_T \Pi(\omega, k_\perp) &= k_\perp^2 \Delta_T \Pi_{\text{tr}}(\omega, k_\perp) + p^2(\omega, k_\perp) \Delta_T \Pi_{00}(\omega, k_\perp) \\ &= \frac{16\alpha}{v_F^2} \int_0^\infty \frac{dq_\perp}{e^{q_\perp/T} + 1} \left[\omega^2 \right. \\ &\quad \left. + \frac{\tilde{p}^2(\omega, k_\perp)}{2} \sum_{\lambda=\pm 1} \frac{W(\omega, k_\perp, q_\perp)}{\tilde{p}(\omega, k_\perp)} + \frac{v_F^2 k_\perp^2}{2} \sum_{\lambda=\pm 1} \frac{\tilde{p}(\omega, k_\perp)}{W(\omega, k_\perp, q_\perp)} \right].\end{aligned}\quad (60)$$

At zero temperature the quantity $\Pi_{00}^{(0)}$ is given by the first line in Eq. (39) and the quantity $\Pi^{(0)}$ is given by

$$\begin{aligned}\Pi^{(0)}(\omega, k_\perp) &= k_\perp^2 \Pi_{\text{tr}}^{(0)}(\omega, k_\perp) + p^2(\omega, k_\perp) \Pi_{00}^{(0)}(\omega, k_\perp) \\ &= -i\pi\alpha k_\perp^2 \tilde{p}(\omega, k_\perp).\end{aligned}\quad (61)$$

We note that at $k_\perp = 0$ the quantity $\Delta_T \Pi_{00}(\omega, 0) = 0$. This is seen from Eqs. (42), (43) and (45) if to take into account that at $\lambda = 1$ $W(\omega, 0, q_\perp) = -\omega - 2q_\perp$ whereas at $\lambda = -1$ $W(\omega, 0, q_\perp) = 2q_\perp - \omega$ holds for any q_\perp . Then, by using Eq. (60), one concludes that $\Delta_T \Pi(\omega, 0) = 0$ as well. As can be seen from Eqs. (39) and (61), the same property $\Pi_{00}^{(0)}(\omega, 0) = \Pi^{(0)}(\omega, 0) = 0$ holds at zero temperature as well.

Now we obtain the asymptotic expression for $\Delta_T \Pi_{00}$ under the condition (59). The main contribution to the integral in the first formula of Eq. (45) is given by $q_\perp \sim T$. Taking into account that $\omega \gg T$ and $\omega \geq k_\perp$, one can conclude that the second and third intervals of q_\perp in Eq. (43) do not contribute to the result essentially. Keeping in mind that for $q_\perp \sim T$

$$\omega - 2q_\perp \approx \omega \gg v_F k_\perp \quad (62)$$

holds, for $\lambda = 1$ from Eq. (42) we obtain

$$W_1 \equiv W(\omega, k_\perp, q_\perp) \approx -(\omega + 2q_\perp) + \frac{v_F^2 k_\perp^2}{2(\omega + 2q_\perp)}.\quad (63)$$

Similarly, from the first line of Eq. (43) we find

$$W_{-1} \equiv W(\omega, k_\perp, q_\perp) \approx -(\omega - 2q_\perp) + \frac{v_F^2 k_\perp^2}{2(\omega - 2q_\perp)}.\quad (64)$$

Taking into account that

$$\frac{1}{\tilde{p}(\omega, k_\perp)} \approx \frac{1}{\omega} \left(1 + \frac{v_F^2 k_\perp^2}{2\omega^2} \right),\quad (65)$$

from Eqs. (63)–(65) one arrives at

$$\frac{1}{2} \frac{W_1 + W_{-1}}{\tilde{p}(\omega, k_\perp)} \approx -1 + \frac{2v_F^2 k_\perp^2 q_\perp^2}{\omega^4}. \quad (66)$$

Substituting Eq. (66) in the first formula of Eq. (45), one obtains the final result for the real part of $\Delta_T \Pi_{00}$:

$$\begin{aligned} \text{Re} \Delta_T \Pi_{00}(\omega, k_\perp) &\approx 32\alpha \frac{k_\perp^2}{\omega^4} \int_0^\infty dq_\perp \frac{q_\perp^2}{e^{q_\perp/T} + 1} \\ &= 48\alpha \zeta(3) \frac{k_\perp^2 T^3}{\omega^4}, \end{aligned} \quad (67)$$

where $\zeta(z)$ is the Riemann zeta function.

In the above, we have neglected by the imaginary part of $\text{Im} \Delta_T \Pi_{00}$ which originates from the second line of Eq. (43). It can be shown, however, that under the condition (59) $\text{Im} \Delta_T \Pi_{00}$ is exponentially small. Really, from the second line of Eq. (43) and the first formula of Eq. (45) we have

$$\text{Im} \Delta_T \Pi_{00}(\omega, k_\perp) = -\frac{8\alpha}{v_F^2 \tilde{p}(\omega, k_\perp)} \int_{(\omega - v_F k_\perp)/2}^{(\omega + v_F k_\perp)/2} dq_\perp \frac{[v_F^2 k_\perp^2 - (2q_\perp - \omega)^2]^{1/2}}{e^{q_\perp/T} + 1}. \quad (68)$$

Introducing the new variable $t = 2q_\perp/(v_F k_\perp)$, this can be represented in the form

$$\begin{aligned} \text{Im} \Delta_T \Pi_{00}(\omega, k_\perp) &= -\frac{4\alpha k_\perp^2}{\tilde{p}(\omega, k_\perp)} \int_{\omega/(v_F k_\perp) - 1}^{\omega/(v_F k_\perp) + 1} \frac{dt}{e^{v_F k_\perp t/(2T)} + 1} \\ &\quad \times \sqrt{1 - \left(t - \frac{\omega}{v_F k_\perp}\right)^2}. \end{aligned} \quad (69)$$

Due to Eq. (62), this is an integration over the narrow interval centered at $\omega/(v_F k_\perp)$. At the ends of this interval the square root in the integrand is equal to zero and in the middle to unity. Thus, the trapezium estimation of the integral results in

$$\text{Im} \Delta_T \Pi_{00}(\omega, k_\perp) \approx -\frac{4\alpha k_\perp^2}{\sqrt{\omega^2 - v_F^2 k_\perp^2}} \frac{1}{e^{\omega/(2T)} + 1} \quad (70)$$

confirming an exponential smallness of the imaginary part of the polarization tensor at high frequencies.

We are coming to calculation of the reflection coefficients and reflectivities of graphene in the scattering region (30). For photons on a mass-shell the condition $k_\perp^2 + k_3^2 = \omega^2$ is satisfied, so that k_\perp can be expressed as

$$k_\perp = \omega \sin \theta_i, \quad (71)$$

where θ_i is the angle of incidence. From Eqs. (39) and (67) we obtain the following expression for the 00-component of the polarization tensor at high frequencies

$$\Pi_{00}(\omega, k_{\perp}) \approx \frac{i\pi\alpha k_{\perp}^2}{\tilde{p}(\omega, k_{\perp})} + 48\alpha\zeta(3)\frac{k_{\perp}^2 T^3}{\omega^4}. \quad (72)$$

Substituting this in Eq. (14) for the TM reflection coefficient and using Eq. (71) and the inequalities $v_F \ll 1$, $T/\omega \ll 1$, one obtains

$$\begin{aligned} r_{\text{TM}}(\omega, \theta_i) &\approx \frac{\pi\alpha \cos \theta_i \left(1 + \frac{v_F^2}{2} \sin^2 \theta_i\right) - 48i\alpha\zeta(3)\frac{T^3}{\omega^3} \cos \theta_i}{2 + \pi\alpha \cos \theta_i \left(1 + \frac{v_F^2}{2} \sin^2 \theta_i\right) - 48i\alpha\zeta(3)\frac{T^3}{\omega^3} \cos \theta_i} \\ &\approx \frac{\pi\alpha \cos \theta_i}{2 + \pi\alpha \cos \theta_i} \left[1 + \frac{v_F^2}{2} \sin^2 \theta_i - i\frac{48\zeta(3)}{\pi} \left(\frac{T}{\omega}\right)^3\right]. \end{aligned} \quad (73)$$

The reflectivity of the TM polarized light from graphene under the condition (59) follows from Eq. (73)

$$|r_{\text{TM}}(\omega, \theta_i)|^2 \approx \frac{\pi^2 \alpha^2 \cos^2 \theta_i}{(2 + \pi\alpha \cos \theta_i)^2} \left[1 + v_F^2 \sin^2 \theta_i + \left(\frac{48\zeta(3)}{\pi}\right)^2 \left(\frac{T}{\omega}\right)^6\right]. \quad (74)$$

Note that the corrections to unity in the square brackets of Eq. (74) are very minor. This is seen from the fact that $v_F^2 = (v_F/c)^2 \approx 10^{-5}$ and $T/\omega = k_B T/(\hbar\omega) \approx 10^{-2}$ at room temperature and optical frequencies. Because of this, in the high frequency region the relative thermal correction to the TM reflectivity of graphene at room temperature is of order 10^{-12} (at zero temperature the result (74) was obtained in Ref. [20]).

In Fig. 3, we plot the TM reflectivity of graphene computed by Eq. (74) as a function of θ_i (the lower line). At the normal incidence ($\theta_i = 0$) we have

$$|r_{\text{TM}}(\omega, 0)|^2 \approx \frac{\pi^2 \alpha^2}{(2 + \pi\alpha)^2} \approx 1.28 \times 10^{-4} \quad (75)$$

in agreement with the result of Ref. [8] obtained numerically using the local model for the conductivity of graphene. As is seen in Fig. 3, at high frequencies the TM reflectivity of graphene is rather small and decreases with increasing angle of incidence.

To consider the TE reflectivity of graphene at high frequencies, we need the asymptotic expression for the quantity $\Delta_T \Pi$ defined in Eq. (60). Substituting Eqs. (63) and (64) in Eq. (60), one obtains

$$\begin{aligned} \text{Re} \Delta_T \Pi(\omega, k_{\perp}) &\approx -32\alpha k_{\perp}^2 \int_0^{\infty} \frac{dq_{\perp}}{e^{q_{\perp}/T} + 1} \frac{q_{\perp}^2}{\omega^2 - q_{\perp}^2} \\ &\approx -32\alpha \frac{k_{\perp}^2}{\omega^2} \int_0^{\infty} \frac{q_{\perp}^2 dq_{\perp}}{e^{q_{\perp}/T} + 1} = -48\alpha\zeta(3)k_{\perp}^2 \frac{T^3}{\omega^2}. \end{aligned} \quad (76)$$

Similar to the case of $\text{Im}\Delta_T\Pi_{00}$, it is easily seen that $\text{Im}\Delta_T\Pi$ is exponentially small.

As a result, the asymptotic expression for Π at high frequencies is obtained from Eqs. (61) and (76)

$$\Pi(\omega, k_\perp) \approx -i\pi\alpha k_\perp^2 \tilde{p}(\omega, k_\perp) - 48\alpha\zeta(3)k_\perp^2 \frac{T^3}{\omega^2}. \quad (77)$$

We substitute this equation in the second line of Eq. (14) and use Eq. (71) and the smallness of our parameters v_F and T/ω :

$$\begin{aligned} r_{\text{TE}}(\omega, \theta_i) &\approx -\frac{\pi\alpha\omega \left(1 - \frac{v_F^2}{2} \sin^2 \theta_i\right) - 48i\alpha\zeta(3)\frac{T^3}{\omega^2}}{2\omega \cos \theta_i + \pi\alpha\omega \left(1 - \frac{v_F^2}{2} \sin^2 \theta_i\right) - 48i\alpha\zeta(3)\frac{T^3}{\omega^2}} \\ &\approx -\frac{\pi\alpha \left(1 - \frac{v_F^2}{2} \sin^2 \theta_i\right)}{2 \cos \theta_i + \pi\alpha} \left[1 - i\frac{48\zeta(3)}{\pi} \left(\frac{T}{\omega}\right)^3\right]. \end{aligned} \quad (78)$$

The reflectivity of the TE polarized light from graphene at high frequencies is given by

$$|r_{\text{TE}}(\omega, \theta_i)|^2 \approx \frac{\pi^2\alpha^2}{(2 \cos \theta_i + \pi\alpha)^2} \left[1 - v_F^2 \sin^2 \theta_i + \left(\frac{48\zeta(3)}{\pi}\right)^2 \left(\frac{T}{\omega}\right)^6\right]. \quad (79)$$

Similar to Eq. (74), the corrections to unity in the square brackets of Eq. (79) are very small. At $T = 0$ the result (79) was derived in Ref. [20].

The TE reflectivity of graphene computed by Eq. (79) as a function of θ_i is shown in Fig. 3 (the upper line). At the normal incidence ($\theta_i = 0$) we have

$$|r_{\text{TE}}(\omega, 0)|^2 = |r_{\text{TM}}(\omega, 0)|^2, \quad (80)$$

where $|r_{\text{TM}}(\omega, 0)|^2$ is given in Eq. (75). This is in agreement with Ref. [8]. However, with increasing angle of incidence, $|r_{\text{TE}}(\omega, \theta_i)|^2$ monotonously increases, as opposite to $|r_{\text{TM}}(\omega, \theta_i)|^2$, which decreases with the increase of θ_i . Thus, at this point our quantitative results disagree with the qualitative conclusion of Ref. [8] that in the framework of the Dirac model $|r_{\text{TE}}(\theta_i)|^2 = |r_{\text{TM}}(0)|^2$ holds for any angle of incidence.

V. REFLECTIVITY OF GRAPHENE AT LOW AND INTERMEDIATE FREQUENCIES

In this section, we derive analytic asymptotic expressions for the polarization tensor and reflectivities of graphene in the scattering frequency interval (30) at low frequencies satisfying

the condition $\omega \ll T$. We also perform numerical computations using the exact expressions for the polarization tensor and find explicitly the application regions for the asymptotic expressions at low and high frequencies.

We start from the imaginary part of the thermal correction $\Delta_T \Pi_{00}$ in the first formula of Eq. (45), which is determined by the second line of Eq. (43)

$$\begin{aligned} \text{Im} \Delta_T \Pi_{00}(\omega, k_\perp) &= -\frac{8\alpha}{v_F^2 \tilde{p}(\omega, k_\perp)} \int_{(\omega - v_F k_\perp)/2}^{(\omega + v_F k_\perp)/2} \frac{dq_\perp}{e^{q_\perp/T} + 1} \sqrt{v_F^2 k_\perp^2 - (\omega - 2q_\perp)^2} \quad (81) \\ &= -\frac{8\alpha}{v_F^2 \tilde{p}(\omega, k_\perp)} \left[\int_{(\omega - v_F k_\perp)/2}^{\omega/2} \frac{dq_\perp}{e^{q_\perp/T} + 1} \sqrt{v_F^2 k_\perp^2 - (\omega - 2q_\perp)^2} \right. \\ &\quad \left. + \int_{\omega/2}^{(\omega + v_F k_\perp)/2} \frac{dq_\perp}{e^{q_\perp/T} + 1} \sqrt{v_F^2 k_\perp^2 - (\omega - 2q_\perp)^2} \right]. \end{aligned}$$

It is convenient to introduce new variables $x = \omega - 2q_\perp$ and $x = 2q_\perp - \omega$ in the first and second integrals on the right-hand side of Eq. (81), respectively. This results in

$$\text{Im} \Delta_T \Pi_{00}(\omega, k_\perp) = -\frac{4\alpha}{v_F^2 \tilde{p}(\omega, k_\perp)} \int_0^{v_F k_\perp} dx \sqrt{v_F^2 k_\perp^2 - x^2} \frac{2 + e^{\frac{\omega+x}{2T}} + e^{\frac{\omega-x}{2T}}}{\left(e^{\frac{\omega-x}{2T}} + 1\right) \left(e^{\frac{\omega+x}{2T}} + 1\right)}. \quad (82)$$

Now we take into account that $x \ll \omega$ because in the scattering region under consideration $v_F k_\perp \ll k_\perp \leq \omega$. In the lowest order one can put $\omega \pm x \approx \omega$ and using the condition $\omega \ll T$ obtain

$$\text{Im} \Delta_T \Pi_{00}(\omega, k_\perp) \approx -\pi\alpha \frac{k_\perp^2}{\tilde{p}(\omega, k_\perp)} \frac{2}{e^{\frac{\omega}{2T}} + 1}. \quad (83)$$

Comparing this result with Eq. (39), we conclude that at low frequencies the thermal correction to Π_{00} gives the same contribution to the imaginary part of Π_{00} as the zero-temperature part $\Pi_{00}^{(0)}$.

The real part of the thermal correction $\Delta_T \Pi_{00}$ is determined by Eq.(42) and by the first and third lines of Eq. (43). Substituting these in the first formula of Eq. (45), one finds

$$\begin{aligned} \text{Re} \Delta_T \Pi_{00}(\omega, k_\perp) &= \frac{16\alpha}{v_F^2} \left[\int_0^\infty \frac{dq_\perp}{e^{q_\perp/T} + 1} - \frac{1}{2\tilde{p}(\omega, k_\perp)} \int_0^\infty dq_\perp \frac{\sqrt{(\omega + 2q_\perp)^2 - v_F^2 k_\perp^2}}{e^{q_\perp/T} + 1} \right. \\ &\quad - \frac{1}{2\tilde{p}(\omega, k_\perp)} \int_0^{(\omega - v_F k_\perp)/2} dq_\perp \frac{\sqrt{(\omega - 2q_\perp)^2 - v_F^2 k_\perp^2}}{e^{q_\perp/T} + 1} \\ &\quad \left. + \frac{1}{2\tilde{p}(\omega, k_\perp)} \int_{(\omega + v_F k_\perp)/2}^\infty dq_\perp \frac{\sqrt{(\omega - 2q_\perp)^2 - v_F^2 k_\perp^2}}{e^{q_\perp/T} + 1} \right]. \quad (84) \end{aligned}$$

In this equation, we make the following identical transformations. The first integral is calculated explicitly. In the second and third integrals we introduce the new variables

$y = \omega + 2q_\perp$ and $y = \omega - 2q_\perp$, respectively. In the fourth integral we introduce the new variable $y = 2q_\perp - \omega$. Then Eq. (84) takes the form

$$\begin{aligned} \text{Re}\Delta_T\Pi_{00}(\omega, k_\perp) = & \frac{16\alpha}{v_F^2} \left[T \ln 2 - \frac{1}{4\tilde{p}(\omega, k_\perp)} \int_\omega^\infty \frac{dy}{e^{(y-\omega)/(2T)} + 1} \sqrt{y^2 - v_F^2 k_\perp^2} \right. \\ & - \frac{1}{4\tilde{p}(\omega, k_\perp)} \int_{v_F k_\perp}^\omega \frac{dy}{e^{(\omega-y)/(2T)} + 1} \sqrt{y^2 - v_F^2 k_\perp^2} \\ & \left. + \frac{1}{4\tilde{p}(\omega, k_\perp)} \int_{v_F k_\perp}^\infty \frac{dy}{e^{(\omega+y)/(2T)} + 1} \sqrt{y^2 - v_F^2 k_\perp^2} \right]. \end{aligned} \quad (85)$$

In the last integral on the right-hand side of Eq. (85) let us separate the integration region $[v_F k_\perp, \infty)$ into two parts: $[v_F k_\perp, \omega]$ and $[\omega, \infty)$. Then we combine the integral over the first part with the second integral on the right-hand side of Eq. (85) and the integral over the second part — with the first. As a result, we have

$$\begin{aligned} \text{Re}\Delta_T\Pi_{00}(\omega, k_\perp) = & \frac{16\alpha}{v_F^2} \left[T \ln 2 + \frac{1}{4\tilde{p}(\omega, k_\perp)} \int_{v_F k_\perp}^\omega dy \sqrt{y^2 - v_F^2 k_\perp^2} \right. \\ & \times \left(\frac{e^{-\omega/(2T)}}{e^{y/(2T)} + e^{-\omega/(2T)}} - \frac{e^{y/(2T)}}{e^{y/(2T)} + e^{\omega/(2T)}} \right) \\ & \left. - \frac{1}{4\tilde{p}(\omega, k_\perp)} \int_\omega^\infty dy \sqrt{y^2 - v_F^2 k_\perp^2} \left(\frac{e^{\omega/(2T)}}{e^{y/(2T)} + e^{\omega/(2T)}} - \frac{e^{-\omega/(2T)}}{e^{y/(2T)} + e^{-\omega/(2T)}} \right) \right]. \end{aligned} \quad (86)$$

This is an exact result which can be used both for numerical computations and for obtaining the asymptotic expressions at low frequency.

It is easily seen that at $\omega \ll T$ the first integral on the right-hand side of Eq. (86) is negligibly small. To see this we expand the quantity in round brackets in powers of small parameters ω/T and y/T and find the leading order term equal to $-y/(4T)$. After integration with respect to y the magnitude of the first integral in Eq. (86) together with its coefficient appears to be $v_F^2 k_\perp^2/(48T)$.

The second integral on the right-hand side of Eq. (86) can be calculated taking into account that $\omega \ll T$ and $v_F k_\perp \ll \omega < y$. Then we can expand in the small parameters $v_F k_\perp/y$ and ω/T . Keeping in mind also that the main contribution to the integral is given by $y \sim T$, we can replace the lower integration limit with zero. Then from Eq. (86) we obtain

$$\begin{aligned} \text{Re}\Delta_T\Pi_{00}(\omega, k_\perp) \approx & \frac{16\alpha}{v_F^2} \left\{ T \ln 2 - \frac{1}{4\omega} \left(1 + \frac{v_F^2 k_\perp^2}{2\omega^2} \right) \right. \\ & \left. \times \frac{\omega}{T} \int_0^\infty y dy \frac{e^{y/(2T)}}{[e^{y/(2T)} + 1]^2} \right\} \end{aligned} \quad (87)$$

and after integration by parts arrive at

$$\text{Re}\Delta_T\Pi_{00}(\omega, k_\perp) \approx -8\alpha T \ln 2 \frac{k_\perp^2}{\omega^2}. \quad (88)$$

Thus, the contribution of the second integral in Eq. (86) is really much larger than that of the first.

As a result, from Eqs. (39), (83) and (88) one obtains the following expression for the 00-component of the polarization tensor at low frequency

$$\Pi_{00}(\omega, k_\perp) = \frac{i\pi\alpha\omega k_\perp^2}{4T\tilde{p}(\omega, k_\perp)} - 8\alpha T \ln 2 \frac{k_\perp^2}{\omega^2}. \quad (89)$$

Now we substitute Eq. (89) in Eq. (14), use Eq. (71) and replace $\tilde{p}(\omega, k_\perp)$ with ω . In the case of low frequencies this replacement is appropriate because the terms of order v_F^2 are much smaller than the thermal correction. Then we have

$$r_{\text{TM}}(\omega, \theta_i) \approx \frac{\pi\alpha\frac{\omega}{8T} \cos \theta_i + 4i\alpha \ln 2 \frac{T}{\omega} \cos \theta_i}{1 + \pi\alpha\frac{\omega}{8T} \cos \theta_i + 4i\alpha \ln 2 \frac{T}{\omega} \cos \theta_i}. \quad (90)$$

From Eq. (90) the reflectivity of the TM polarized light from graphene at low frequencies is given by

$$|r_{\text{TM}}(\omega, \theta_i)|^2 \approx \frac{\pi^2\alpha^2\frac{\omega^2}{64T^2} \cos^2 \theta_i + 16\alpha^2 \ln^2 2 \frac{T^2}{\omega^2} \cos^2 \theta_i}{\left(1 + \pi\alpha\frac{\omega}{8T} \cos \theta_i\right)^2 + 16\alpha^2 \ln^2 2 \frac{T^2}{\omega^2} \cos^2 \theta_i}. \quad (91)$$

Note that at low frequency both real and imaginary parts of the Π_{00} component (89) contribute to the reflection coefficient (90) and reflectivity (91). The thermal correction contributes essentially to both quantities. At the normal incidence we have

$$|r_{\text{TM}}(\omega, 0)|^2 \approx \frac{\pi^2\alpha^2\frac{\omega^2}{64T^2} + 16\alpha^2 \ln^2 2 \frac{T^2}{\omega^2}}{\left(1 + \pi\alpha\frac{\omega}{8T}\right)^2 + 16\alpha^2 \ln^2 2 \frac{T^2}{\omega^2}}. \quad (92)$$

In Fig. 4, we plot the reflectivity of graphene (92) at $\theta_i = 0$ as a function of frequency measured in K at three different temperatures $T = 10$ K, 100 K, and 300 K (the lower, middle, and upper lines, respectively). As is seen in Fig. 4, at $\omega = 0$ the reflectivity is equal to unity and decreases monotonously with increasing frequency. The comparison with the results of numerical computations (see below) shows that even at the lowest considered temperature $T = 10$ K the asymptotic expression (92) is rather precise. Our analytic results of Fig 4 obtained using the polarization tensor are in rather good agreement with the computational results of Ref. [7] (see their Fig. 2, left) found using the local model for the conductivity

of graphene. Note, however, that with decreasing temperature the local model supposedly overestimates the TM reflectivity of graphene.

We are coming now to the calculation of the TE reflectivity of graphene at low frequency. Besides Π_{00} , the reflection coefficient r_{TE} in Eq. (14) is expressed via the quantity Π defined in Eqs. (60) and (61). To calculate $\Delta_T \Pi$ at $\omega \ll T$, it is convenient to use its definition in the first line of Eq. (60) and already obtained results (83) and (88) for $\Delta_T \Pi_{00}$. The quantity $\Delta_T \Pi_{\text{tr}}$ is given in the second formula of Eq. (45). Both its imaginary and real parts at low frequency are calculated using the same procedure, as was applied above in this section to calculate $\text{Im} \Delta_T \Pi_{00}$ and $\text{Re} \Delta_T \Pi_{00}$. The results are

$$\begin{aligned} \text{Im} \Delta_T \Pi_{\text{tr}}(\omega, k_{\perp}) &\approx \pi \alpha \frac{p^2(\omega, k_{\perp}) + \tilde{p}^2(\omega, k_{\perp})}{\tilde{p}(\omega, k_{\perp})} \frac{2}{e^{\frac{\omega}{2T}} + 1}, \\ \text{Re} \Delta_T \Pi_{\text{tr}}(\omega, k_{\perp}) &\approx 8\alpha T \ln 2 \frac{p^2(\omega, k_{\perp}) + \tilde{p}^2(\omega, k_{\perp}) + 2v_{\text{F}}^2 k_{\perp}^2}{\omega^2}. \end{aligned} \quad (93)$$

Then from the second line of Eq. (39) and Eq. (93) one finds

$$\begin{aligned} \Pi_{\text{tr}} &\approx 8\alpha T \ln 2 \frac{p^2(\omega, k_{\perp}) + \tilde{p}^2(\omega, k_{\perp}) + 2v_{\text{F}}^2 k_{\perp}^2}{\omega^2} \\ &\quad + i \frac{\omega}{4T} \pi \alpha \frac{p^2(\omega, k_{\perp}) + \tilde{p}^2(\omega, k_{\perp})}{\tilde{p}(\omega, k_{\perp})}. \end{aligned} \quad (94)$$

Finally, from Eqs. (89) and (94) we arrive at

$$\Pi(\omega, k_{\perp}) \approx 8\alpha T \ln 2 k_{\perp}^2 - i \frac{\omega}{4T} \pi \alpha k_{\perp}^2 \tilde{p}(\omega, k_{\perp}), \quad (95)$$

where we have taken into account that $v_{\text{F}}^2 k_{\perp}^2 \ll \omega^2$.

Substituting Eq. (95) in Eq. (14) for the TE reflection coefficient, using Eq. (71) and taking into account that $\tilde{p}(\omega, k_{\perp}) \approx \omega$ in the scattering frequency interval, one obtains

$$r_{\text{TE}}(\omega, \theta_i) = - \frac{\pi \alpha \frac{\omega}{8T} + 4i \alpha \ln 2 \frac{T}{\omega}}{\cos \theta_i + \pi \alpha \frac{\omega}{8T} + 4i \alpha \ln 2 \frac{T}{\omega}}. \quad (96)$$

The reflectivity of the TE polarized light from graphene at low frequencies is given by

$$|r_{\text{TE}}(\omega, \theta_i)|^2 = \frac{\pi^2 \alpha^2 \frac{\omega^2}{64T^2} + 16\alpha^2 \ln^2 2 \frac{T^2}{\omega^2}}{(\cos \theta_i + \pi \alpha \frac{\omega}{8T})^2 + 16\alpha^2 \ln^2 2 \frac{T^2}{\omega^2}}. \quad (97)$$

From the comparison of Eq. (97) with Eq. (92) it is seen that at the normal incidence

$$|r_{\text{TE}}(\omega, 0)|^2 = |r_{\text{TM}}(\omega, 0)|^2, \quad (98)$$

as it should be, where the right-hand side of this equation is given by Eq. (92). Thus, Fig. 4 demonstrating dependence of the reflectivity of graphene on frequency at the normal incidence is equally applicable to both TM and TE polarized light.

Now we illustrate dependence of the reflectivities of graphene at low frequency on the angle of incidence. Calculations were performed using Eqs. (91) and (97) for the TM and TE polarized light, respectively. In Fig. 5 the calculation results are presented by the upper pair of solid lines computed at $\omega/T = 0.01$ and lower pair corresponding to $\omega/T = 0.03$. As is seen from Fig. 5, at low frequencies the reflectivities of TM polarized light decrease with increasing θ_i , whereas the reflectivities of TE polarized light are the monotonously increasing functions of θ_i . In this sense the dependence of reflectivities of graphene at low frequencies on the angle of incidence is similar to that at high frequencies. The single difference is that the magnitudes of reflectivity at low frequencies are several orders of magnitude higher than at high frequencies.

In the end of this section we present the results of numerical computations for the reflectivity of graphene over a wide range of frequencies and compare them with the analytic asymptotic results obtained in this and previous sections. As an example, we choose the incidence angle $\theta_i = 30^\circ$ and perform numerical computations of the TM and TE reflectivities as functions of ω/T in the wide range from 10^{-3} to 10^3 . Let us start from the TM polarized light. In this case computations are done using Eqs. (14), (19), (43) and (45). The computational results are shown by the solid line in Fig. 6(a) plotted in the double logarithmic scale. In the same figure, the long-dashed line shows the analytic asymptotic results at high frequencies. They are calculated using Eq. (74) at $\theta = 30^\circ$. The analytic asymptotic results at low frequencies are calculated by Eq. (91) and shown by the short-dashed line. As is seen in Fig. 6(a), the analytic asymptotic results are in a very good agreement with the results of numerical computations over a wide frequency region. Thus, at low frequencies the relative deviation of the short-dashed line less than 5% occurs at all $\omega/T < 0.3$ [$\log(\omega/T) < -0.52$]. At high frequencies less than 5% relative deviation holds at all $\omega/T > 9$ [$\log(\omega/T) > 0.95$].

Finally we consider the TE polarized light incident on graphene at the same angle $\theta_i = 30^\circ$. We perform numerical computations using Eqs. (14), (43), (60) and (61). In Fig. 6(b), the computational results are presented by the solid line plotted in the double logarithmic scale. Similar to Fig. 6(a), the analytic results of Eq. (79) at high frequencies are shown by the long-dashed line and the analytic results of Eq. (97) at low frequencies are shown by

the short-dashed line. From Fig. 6(b) it is seen that at low frequencies less than 5% relative deviation occurs at $\omega/T < 0.25$ [$\log(\omega/T) < -0.6$], and at high frequencies less than 5% relative deviation holds at all $\omega/T > 9$ [$\log(\omega/T) > 0.95$]. This solves the question when one can use simple asymptotic formulas and when more cumbersome numerical computations are necessary.

VI. CONCLUSIONS AND DISCUSSION

In the foregoing, we have developed quantum field theoretical description for the reflectivity of graphene described in the framework of the Dirac model. This description exploits the polarization tensor of graphene at nonzero temperature in (2+1)-dimensional space-time. The previously known representation of this tensor [10] obtained in thermal quantum field theory in Matsubara formulation is applicable only at the imaginary Matsubara frequencies and does not admit physically reasonable analytic continuation to the real frequency axis. Here we derive another representation for the polarization tensor of graphene which possesses the required analytic properties over the entire plane of complex frequencies. At zero temperature our polarization tensor coincides with that obtained in Ref. [9]. At nonzero temperature our tensor takes the same values as the one obtained in Ref. [10] at all Matsubara frequencies. This justifies all numerous applications of the polarization tensor of Ref. [10] to calculation of the Casimir interaction in systems including graphene and graphene-coated substrates [10–17]. However, as shown in this paper, the polarization tensor of Ref. [10] is an oscillating function along the imaginary frequency axis, and this precludes the use of its analytic continuation to real frequency axis for theoretical description of the reflectivity of graphene. On the contrary, in the representation obtained here the polarization tensor is a monotonously decreasing function of the imaginary frequency and admits the analytic continuation to real frequency axis satisfying all physical requirements.

Using the derived representation for the polarization tensor at nonzero temperature, we have obtained analytic expressions for the reflection coefficients and reflectivities of graphene for two independent polarizations of the electromagnetic field in the asymptotic regions of high and low frequencies, as compared to temperature. For the transverse magnetic (p polarized) light our results are in a good agreement with those previously obtained at high [8] and low [7] frequencies using the local model for the conductivity of graphene. However,

some qualitative conclusions about the reflectivity of TE (s polarized) light made previously are not supported by our exact calculations. We have investigated dependences of the TM and TE reflectivities of graphene as functions of frequency and incidence angle. In the latter case it was shown that the TM reflectivity is a decreasing function of the incidence angle, whereas the TE reflectivity increases with increase of the angle of incidence.

Furthermore, we have performed numerical computations of the TM and TE reflectivities of graphene over the wide frequency range. By comparing the analytic and computational results the application regions for the asymptotic expansions at low and high frequencies were determined. It was shown that simple analytic expressions for the reflectivity of graphene obtained here produce very accurate results in the wide regions of frequencies and temperatures.

By and large the developed formalism solves the problem of the reflectivity of pristine (gapless) graphene and graphene characterized by some nonzero mass-gap parameter. In future it would be interesting to generalize this formalism to the case of nonzero chemical potential and consider applications to doped graphene sheets.

Appendix A: Polarization tensor in (2+1)-dimensions at nonzero temperature

In this Appendix, we display the details for the calculation of the polarization tensor of graphene at nonzero temperature. By making the replacement (6) in Eq. (4), we represent the polarization tensor in the form

$$\Pi^{\mu\nu}(i\xi_l, \mathbf{k}_\perp) = \Pi^{\mu\nu}(k) = -8\pi\alpha T \sum_{n=-\infty}^{\infty} \int \frac{d\mathbf{q}_\perp}{(2\pi)^2} \text{tr} S(q) \tilde{\gamma}^\mu S(q-k) \tilde{\gamma}^\nu, \quad (\text{A1})$$

where the spinor propagator is given by

$$S(q) = \frac{1}{i\not{q} - m} = \frac{i\not{q} + m}{q^2 - m^2 - i0} \quad (\text{A2})$$

and the notations introduced in Eqs. (5) and (6) are used here and below.

By calculating the trace over the γ -matrices, we get

$$\Pi^{\mu\nu}(k) = -\frac{32\pi\alpha}{v_F^2} T \sum_{n=-\infty}^{\infty} \int \frac{d\mathbf{q}_\perp}{(2\pi)^2} \frac{Z^{\mu\nu}(k, q)}{R(k, q)}, \quad (\text{A3})$$

where

$$\begin{aligned}
Z^{\mu\nu}(k, q) &= \eta_{\mu'}^{\mu} \eta_{\nu'}^{\nu} \left[q^{\mu'} (q^{\nu'} - \tilde{k}^{\nu'}) + (q^{\mu'} - \tilde{k}^{\mu'}) q^{\nu'} \right. \\
&\quad \left. - q_{\alpha} (q^{\alpha} - \tilde{k}^{\alpha}) g^{\mu'\nu'} + m^2 g^{\mu'\nu'} \right], \\
R(k, q) &= (q_{\mu} q^{\mu} - m^2 + i0) \left[(q_{\mu} - \tilde{k}_{\mu}) (q^{\mu} - \tilde{k}^{\mu}) - m^2 + i0 \right].
\end{aligned} \tag{A4}$$

In there equations, $\tilde{k}^{\mu} \equiv (ik_{l4}, v_F \mathbf{k}_{\perp})$ and $g^{\mu\nu}$ is the metric tensor in (2+1)-dimensions with $g^{00} = -g^{11} = -g^{22} = 1$. Note also that we have made the substitution $\mathbf{q}_{\perp} \rightarrow \mathbf{q}_{\perp}/v_F$ in the integration in Eq. (A1).

For the independent quantities (9) characterizing the polarization tensor at any temperature it follows

$$\Pi_{00(\text{tr})}(k) = -\frac{32\pi\alpha}{v_F^2} T \sum_{n=-\infty}^{\infty} \int \frac{d\mathbf{q}_{\perp}}{(2\pi)^2} \frac{Z_{00(\text{tr})}(k, q)}{R(k, q)}. \tag{A5}$$

Here, by using Eq. (A4), we obtain

$$\begin{aligned}
Z_{00}(k, q) &= -q_{4n}(q_{4n} - k_{4l}) + \mathbf{q}_{\perp}(\mathbf{q}_{\perp} - v_F \mathbf{k}_{\perp}) + m^2, \\
Z_{\text{tr}}(k, q) &= -(1 - 2v_F^2)q_{4n}(q_{4n} - k_{4l}) + \mathbf{q}_{\perp}(\mathbf{q}_{\perp} - v_F \mathbf{k}_{\perp}) \\
&\quad + (1 + 2v_F^2)m^2, \\
R(q, k) &= [q_{4n}^2 + \Gamma^2(q_{\perp})] \left[(q_{4n}^2 - k_{4l}^2) + \tilde{\Gamma}^2(\mathbf{k}_{\perp}, \mathbf{q}_{\perp}) \right],
\end{aligned} \tag{A6}$$

where $\Gamma(q_{\perp})$ is defined in Eq. (22) and

$$\tilde{\Gamma}(\mathbf{k}_{\perp}, \mathbf{q}_{\perp}) = [(\mathbf{q}_{\perp} - v_F \mathbf{k}_{\perp})^2 + m^2]^{1/2}. \tag{A7}$$

We mention that Π_{00} in (A5) coincides up to an overall factor with Eq. (A3) in Ref. [28].

Now, following the idea behind the Abel-Plana formula (see, e.g., Ref. [25]), we represent the Matsubara sum over n in Eq. (A5) as an integral in the complex q_4 plane,

$$\Pi_{00(\text{tr})}(k) = \frac{32\pi\alpha}{v_F^2} \int_{\gamma_1 \cup \gamma_2} \frac{dq_4}{2\pi} \int \frac{d\mathbf{q}_{\perp}}{(2\pi)^2} \frac{1}{e^{iq_4/T} + 1} \frac{Z_{00(\text{tr})}(k, q)}{R(k, q)}, \tag{A8}$$

where the integration path $\gamma_1 \cup \gamma_2$ encircles the poles of the real axis at the fermionic Matsubara frequencies indicated by dots (see Fig. 7). In the same figure, the zeros of the quantity $R(q, k)$ in the denominator of (A8) at $q_4 = \pm i\Gamma$ and $q_4 = \pm i\tilde{\Gamma} + k_{4l}$ are shown as crosses.

It is convenient to represent Eq. (A8) as the sum of two integrals. The first of them is along the path γ_1 and the second is along the path γ_2 . In order to have a decreasing function in the upper half plane under the integral along the path γ_1 , we use the identity

$$\frac{1}{e^{iq_4/T} + 1} = 1 - \frac{1}{e^{-iq_4/T} + 1}. \quad (\text{A9})$$

We substitute Eq. (A9) in the first integral of Eq. (A8) along the path γ_1 . In so doing the unity results in the polarization tensor at zero temperature

$$\begin{aligned} \Pi_{00(\text{tr})}^{(0)}(k) &= \frac{32\pi\alpha}{v_F^2} \int_{\gamma_1} \frac{dq_4}{2\pi} \int \frac{d\mathbf{q}_\perp}{(2\pi)^2} \frac{Z_{00(\text{tr})}(k, q)}{R(k, q)} \\ &= -\frac{32\pi\alpha}{v_F^2} \int_{-\infty}^{\infty} \frac{dq_4}{2\pi} \int \frac{d\mathbf{q}_\perp}{(2\pi)^2} \frac{Z_{00(\text{tr})}(k, q)}{R(k, q)}. \end{aligned} \quad (\text{A10})$$

The substitution of the second term of Eq. (A9) in the first integral of Eq. (A8) along the path γ_1 together with the second integral of Eq. (A8) along the path γ_2 result in the thermal correction to the polarization tensor

$$\begin{aligned} \Delta_T \Pi_{00(\text{tr})}(k) &= -\frac{32\pi\alpha}{v_F^2} \int_{\gamma_1} \frac{dq_4}{2\pi} \int \frac{d\mathbf{q}_\perp}{(2\pi)^2} \frac{1}{e^{-iq_4/T} + 1} \frac{Z_{00(\text{tr})}(k, q)}{R(k, q)} \\ &+ \frac{32\pi\alpha}{v_F^2} \int_{\gamma_2} \frac{dq_4}{2\pi} \int \frac{d\mathbf{q}_\perp}{(2\pi)^2} \frac{1}{e^{iq_4/T} + 1} \frac{Z_{00(\text{tr})}(k, q)}{R(k, q)}. \end{aligned} \quad (\text{A11})$$

It is well known that the polarization tensor has no ultraviolet divergencies in (2+1)-dimensions. In fact, its divergence degree is +1, which would correspond to a linear divergence. The latter, however, is not present due to the gauge invariance. Otherwise, the linear divergence would reside in the zero-temperature part $\Pi_{00(\text{tr})}^{(0)}$. The thermal corrections $\Delta_T \Pi_{00(\text{tr})}$ do not have any ultraviolet divergencies, which is evident due to the Boltzmann factors.

Calculation of the polarization tensor at zero temperature (A10) was performed in Ref. (10) with the result (19). Now we calculate the thermal correction to it (A11). For this purpose, we close the integration pathes γ_1 and γ_2 by the half circles of infinitely large radii in the upper and lower half planes, respectively. These circles do not contribute to the result which is given by the corresponding residua in the poles of both integrands shown in

Fig. 7 as crosses

$$\begin{aligned} \Delta_T \Pi_{00(\text{tr})}(k) = & \frac{32\pi\alpha}{v_F^2} \int \frac{d\mathbf{q}_\perp}{(2\pi)^2} \sum_{\lambda=\pm 1} \left\{ \frac{1}{e^{\Gamma(q_\perp)/T} + 1} \right. \\ & \frac{Z_{00(\text{tr})}(k, i\lambda\Gamma(q_\perp), \mathbf{q}_\perp)}{2\lambda\Gamma(q_\perp)[(i\lambda\Gamma(q_\perp) - k_{4l})^2 + \tilde{\Gamma}^2(\mathbf{k}_\perp, \mathbf{q}_\perp)]} \\ & \left. + \frac{1}{e^{[-i\lambda k_{4l} + \tilde{\Gamma}(\mathbf{k}_\perp, \mathbf{q}_\perp)/T] + 1}} \frac{Z_{00(\text{tr})}(k, k_{4l} + i\lambda\tilde{\Gamma}(\mathbf{k}_\perp, \mathbf{q}_\perp), \mathbf{q}_\perp)}{2\lambda\tilde{\Gamma}(\mathbf{k}_\perp, \mathbf{q}_\perp)[(i\lambda\tilde{\Gamma}(\mathbf{k}_\perp, \mathbf{q}_\perp) + k_{4l})^2 + \Gamma^2(q_\perp)]} \right\}, \end{aligned} \quad (\text{A12})$$

where the contributions with $\lambda = 1$ come from the upper half plane and those with $\lambda = -1$ from the lower half plane.

Equation (A12) can be simplified taking into account that according to Eq. (7) k_{4l} are the Matsubara frequencies and, thus, $\exp(-i\lambda k_{4l}/T) = 1$. In fact doing just this way is necessary for a correct analytic continuation to non-Matsubara frequencies since otherwise the replacement $k_{4l} \rightarrow i\omega$ would not result in a function (A12) decreasing for $\omega \rightarrow \pm\infty$ as is required for the analytic continuation. In application to temperature Green functions this was first mentioned in Ref. [21] and extensively elaborated in Ref. [22]. A recent, mathematically equivalent, treatment can be found in Ref. [28] [see Eq. (A5) there]. Further we use the symmetry of the integrand under the substitution $\mathbf{q}_\perp \rightarrow v_F \mathbf{k}_\perp - \mathbf{q}_\perp$ and making the replacement $\lambda \rightarrow -\lambda$ in the second term of Eq. (A12) we arrive at

$$\begin{aligned} \Delta_T \Pi_{00(\text{tr})}(k) = & \frac{16\pi\alpha}{v_F^2} \int \frac{d\mathbf{q}_\perp}{(2\pi)^2} \frac{1}{\Gamma(q_\perp)} \frac{1}{e^{\Gamma(q_\perp)/T} + 1} \\ & \times \sum_{\lambda=\pm 1} \frac{Z_{00(\text{tr})}(k, i\lambda\Gamma(q_\perp), \mathbf{q}_\perp) + Z_{00(\text{tr})}(k, k_{4l} - i\lambda\Gamma(q_\perp), v_F \mathbf{k}_\perp - \mathbf{q}_\perp)}{[k_{4l} - i\lambda\Gamma(q_\perp)]^2 + \tilde{\Gamma}^2(\mathbf{k}_\perp, \mathbf{q}_\perp)}. \end{aligned} \quad (\text{A13})$$

As said above, in this representation, the analytic continuation of $\Delta_T \Pi_{00(\text{tr})}$ from the Matsubara frequencies k_{4l} to any frequency $k_4 \equiv \omega$, including the real frequency axis, can be done directly.

Using the polar coordinates ($q_\perp = |\mathbf{q}_\perp| = \sqrt{q_1^2 + q_2^2}, \varphi$) in the \mathbf{q}_\perp -plane, it is possible to perform one of the two integrations in Eq. (A13). Taking into account that

$$2\mathbf{q}_\perp \mathbf{k}_\perp = 2q_\perp k_\perp \cos \varphi, \quad (\text{A14})$$

for the quantity in the denominator of (A13) we obtain

$$[k_{4l} - i\lambda\Gamma(q_\perp)]^2 + \tilde{\Gamma}^2(\mathbf{k}_\perp, \mathbf{q}_\perp) = Q(k_{4l}, k_\perp, q_\perp) - 2v_F q_\perp k_\perp \cos \varphi \quad (\text{A15})$$

with the notation

$$Q(k_{4l}, k_{\perp}, q_{\perp}) = k_{4l}^2 + v_F^2 k_{\perp}^2 - 2i\lambda k_{4l}\Gamma(q_{\perp}). \quad (\text{A16})$$

In the numerator of Eq. A13) we get

$$\begin{aligned} & Z_{00(\text{tr})}(k, i\lambda\Gamma(q_{\perp}), \mathbf{q}_{\perp}) + Z_{00(\text{tr})}(k, k_{4l} - i\lambda\Gamma(q_{\perp}), v_F \mathbf{k}_{\perp} - \mathbf{q}_{\perp}) \\ &= Q(k_{4l}, k_{\perp}, q_{\perp}) - 2v_F q_{\perp} k_{\perp} \cos \varphi + M_{00(\text{tr})}(k_{4l}, k_{\perp}, q_{\perp}) \end{aligned} \quad (\text{A17})$$

with

$$\begin{aligned} M_{00}(k_{4l}, k_{\perp}, q_{\perp}) &= -(k_{4l}^2 + v_F^2 k_{\perp}^2) + 4i\lambda k_{4l}\Gamma(q_{\perp}) + 4\Gamma^2(q_{\perp}), \\ M_{\text{tr}}(k_{4l}, k_{\perp}, q_{\perp}) &= -(k_{4l}^2 + v_F^2 k_{\perp}^2) + 4v_F^2 m^2 \\ &\quad + 4(1 - v_F^2)i\lambda k_{4l}\Gamma(q_{\perp}) + 4(1 - v_F^2)\Gamma^2(q_{\perp}). \end{aligned} \quad (\text{A18})$$

Rewriting the integral (A13) in the polar coordinates and using Eqs. (A15) and (A17), we obtain

$$\begin{aligned} \Delta_T \Pi_{00(\text{tr})}(k) &= \frac{16\pi\alpha}{v_F^2} \int_0^{\infty} dq_{\perp} \frac{q_{\perp}}{\Gamma(q_{\perp})} \frac{1}{e^{\Gamma(q_{\perp})/T} + 1} \\ &\times \left[1 + \sum_{\lambda=\pm 1} \int_0^{2\pi} \frac{d\varphi}{2\pi} \frac{M_{00(\text{tr})}(k_{4l}, k_{\perp}, q_{\perp})}{Q(k_{4l}, k_{\perp}, q_{\perp}) - 2v_F q_{\perp} k_{\perp} \cos \varphi} \right]. \end{aligned} \quad (\text{A19})$$

The remaining angular integral can be carried out by using the formula

$$\int_0^{2\pi} \frac{d\varphi}{2\pi} \frac{1}{Q - a \cos \varphi} = \frac{1}{\sqrt{Q^2 - a^2}} \quad (\text{A20})$$

with $a \equiv 2v_F q_{\perp} k_{\perp}$. Here, the branch of the square root must be defined such that the sign of the imaginary part of the root $\sqrt{Q^2 - a^2}$ be the same as that of Q . This prescription holds for Q as given by Eq. (A16) with real k_{4l} . For a complex k_4 one needs to use the corresponding analytic continuation. Substituting Eq. (A20) in Eq. (A19) and using the notation

$$N(k_{4l}, k_{\perp}, q_{\perp}) = [Q^2(k_{4l}, k_{\perp}, q_{\perp}) - (2v_F q_{\perp} k_{\perp})^2]^{1/2}, \quad (\text{A21})$$

one arrives to the final result (21) for the polarization tensor of graphene defined at the imaginary Matsubara frequencies. The analytic continuation of this tensor to the real frequency axis is described in Sec. II.

[1] M. I. Katsnelson, *Graphene: Carbon in Two Dimensions* (Cambridge University Press, Cambridge, 2012).

- [2] A. H. Castro Neto, F. Guinea, N. M. R. Peres, K. S. Novoselov, and A. K. Geim, *Rev. Mod. Phys.* **81**, 109 (2009).
- [3] M. I. Katsnelson, K. S. Novoselov, and A. K. Geim, *Nature Phys.* **2**, 620 (2006).
- [4] D. Allor, T. D. Cohen, and D. A. McGady, *Phys. Rev. D* **78**, 096009 (2008).
- [5] C. G. Beneventano, P. Giacconi, E. M. Santangelo, and R. Soldati, *J. Phys. A: Math. Theor.* **42**, 275401 (2009).
- [6] G. L. Klimchitskaya and V. M. Mostepanenko, *Phys. Rev. D* **87**, 125011 (2013).
- [7] L. A. Falkovsky and S. S. Pershoguba, *Phys. Rev. B* **76**, 153410 (2007).
- [8] T. Stauber, N. M. R. Peres, and A. K. Geim, *Phys. Rev. B* **78**, 085432 (2008).
- [9] M. Bordag, I. V. Fialkovsky, D. M. Gitman, and D. V. Vassilevich, *Phys. Rev. B* **80**, 245406 (2009).
- [10] I. V. Fialkovsky, V. N. Marachevsky, and D. V. Vassilevich, *Phys. Rev. B* **84**, 035446 (2011).
- [11] M. Bordag, G. L. Klimchitskaya, and V. M. Mostepanenko, *Phys. Rev. B* **86**, 165429 (2012).
- [12] M. Chaichian, G. L. Klimchitskaya, V. M. Mostepanenko, and A. Tureanu, *Phys. Rev. A* **86**, 012515 (2012).
- [13] G. L. Klimchitskaya and V. M. Mostepanenko, *Phys. Rev. B* **87**, 075439 (2013).
- [14] G. L. Klimchitskaya, V. M. Mostepanenko, and Bo E. Sernelius, *Phys. Rev. B* **89**, 125407 (2014).
- [15] G. L. Klimchitskaya, U. Mohideen, and V. M. Mostepanenko, *Phys. Rev. B* **89**, 115419 (2014).
- [16] G. L. Klimchitskaya and V. M. Mostepanenko, *Phys. Rev. A* **89**, 052512 (2014).
- [17] G. L. Klimchitskaya and V. M. Mostepanenko, *Phys. Rev. A* **89**, 062508 (2014).
- [18] G. Gómez-Santos, *Phys. Rev. B* **80**, 245424 (2009).
- [19] A. J. Niemi and G. W. Semenoff, *Ann. Phys. (N.Y.)* **152**, 105 (1984).
- [20] G. L. Klimchitskaya, V. M. Mostepanenko, and V. M. Petrov, In: *Internet of Things, Smart Spaces, and Next Generation Networks and Systems*. Eds.: S. Balandin, S. Andreev, and Y. Koucheryavy (Springer, Cham, 2014), pp. 451–458.
- [21] G. Baym and N. D. Mermin, *J. Math. Phys.* **2**, 232 (1961).
- [22] E. S. Fradkin, *Methods of Green's functions in quantum field theory in quantum statistics*. In: *Quantum Field Theory and Hydrodynamics*, Proc. P. N. Lebedev Physics Institute, vol. 29, edited by D. V. Skobel'tsyn (Consultants Bureau, New York, 1967), pp. 1–131.
- [23] E. Gorbar, V. Gusynin, V. Miransky, and I. Shovkovy, *Phys. Rev. B* **66**, 045108 (2002).

TABLE I: The normalized values of the thermal correction to the 00-component of polarization tensor of graphene computed at the Matsubara frequencies with different numbers (column 1) using the representation of Ref. [10] (column 2) and in this paper (column 3) at $k_{\perp} = 10\xi_1$. The relative thermal correction is given in column 4.

l	$\Delta_T \Pi_{00}^{(a)}/C$	$\Delta_T \Pi_{00}/C$	$\Delta_T \Pi_{00}/\Pi_{00}^{(0)} (\%)$
1	$5.60604848904 \times 10^{-5}$	$5.60604848906 \times 10^{-5}$	4.09
2	$5.0366515197 \times 10^{-6}$	$5.0366515198 \times 10^{-6}$	0.73
3	$1.1114739021 \times 10^{-6}$	$1.1114739022 \times 10^{-6}$	0.24
4	$3.6872960104 \times 10^{-7}$	$3.6872960109 \times 10^{-7}$	0.108
5	$1.547382154 \times 10^{-7}$	$1.547382155 \times 10^{-7}$	0.056
6	$7.56717034 \times 10^{-8}$	$7.56717035 \times 10^{-8}$	0.033
7	$4.12036077 \times 10^{-8}$	$4.12036078 \times 10^{-8}$	0.021
8	$2.42932778 \times 10^{-8}$	$2.42932779 \times 10^{-8}$	0.014
9	$1.52276095 \times 10^{-8}$	$1.52276096 \times 10^{-8}$	0.010
10	$1.00201160 \times 10^{-8}$	$1.00201159 \times 10^{-8}$	0.0073
11	$6.85884188 \times 10^{-9}$	$6.85884190 \times 10^{-9}$	0.0055

- [24] A. I. Akhiezer and V. B. Berestetskii, *Quantum Electrodynamics* (Interscience, New York, 1965).
- [25] M. Bordag, G. L. Klimchitskaya, U. Mohideen, and V. M. Mostepanenko, *Advances in the Casimir Effect* (Oxford University Press, Oxford, 2009).
- [26] G. L. Klimchitskaya, U. Mohideen, and V. M. Mostepanenko, Rev. Mod. Phys. **81**, 1827 (2009).
- [27] V. N. Marachevsky, J. Phys.: Conf. Series **14**, 435 (2012).
- [28] P. K. Pyatkovskiy, J. Phys.: Condens. Matter **21**, 025506 (2009).

TABLE II: The normalized values of the thermal correction (47) to the combination of the components of polarization tensor of graphene computed at the Matsubara frequencies with different numbers (column 1) using the representation of Ref. [10] (column 2) and in this paper (column 3) at $k_{\perp} = 10\xi_1$. The relative thermal correction is given in column 4.

l	$\Delta_T \Pi^{(a)}/D$	$\Delta_T \Pi/D$	$\Delta_T \Pi/\Pi^{(0)} (\%)$
1	$1.12028612025 \times 10^{-4}$	$1.12028612024 \times 10^{-4}$	4.08
2	$4.02785688588 \times 10^{-5}$	$4.02785688597 \times 10^{-5}$	0.73
3	$2.0002626999 \times 10^{-5}$	$2.0002626997 \times 10^{-5}$	0.24
4	$1.1797934387 \times 10^{-5}$	$1.1797934384 \times 10^{-5}$	0.108
5	$7.736289303 \times 10^{-6}$	$7.736289297 \times 10^{-6}$	0.056
6	$5.44805008 \times 10^{-6}$	$5.44805006 \times 10^{-6}$	0.033
7	$4.03778027 \times 10^{-6}$	$4.03778024 \times 10^{-6}$	0.021
8	$3.10943615 \times 10^{-6}$	$3.10943614 \times 10^{-6}$	0.014
9	$2.466807364 \times 10^{-6}$	$2.466807362 \times 10^{-6}$	0.010
10	$2.00397985 \times 10^{-6}$	$2.00397988 \times 10^{-6}$	0.0073
11	$1.65980994 \times 10^{-6}$	$1.65980992 \times 10^{-6}$	0.0055

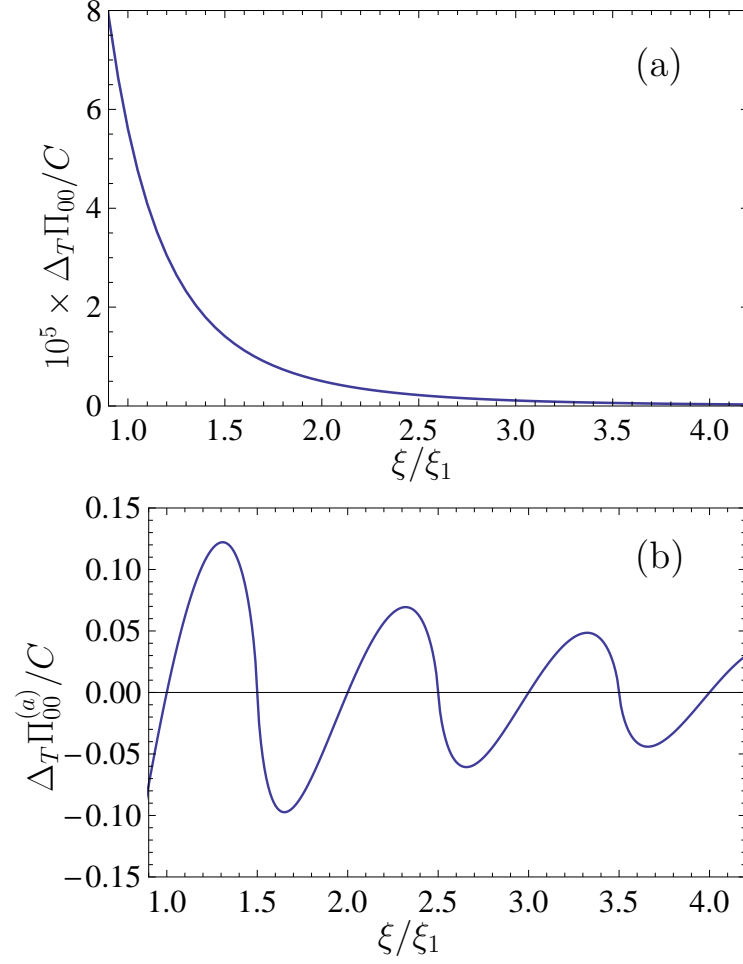


FIG. 1: (Color online) The normalized values of the thermal correction to the 00-component of the polarization tensor of graphene computed as functions of imaginary frequency at $k_{\perp} = 10\xi_1$ (a) in this paper and (b) using the representation of Ref. [10].

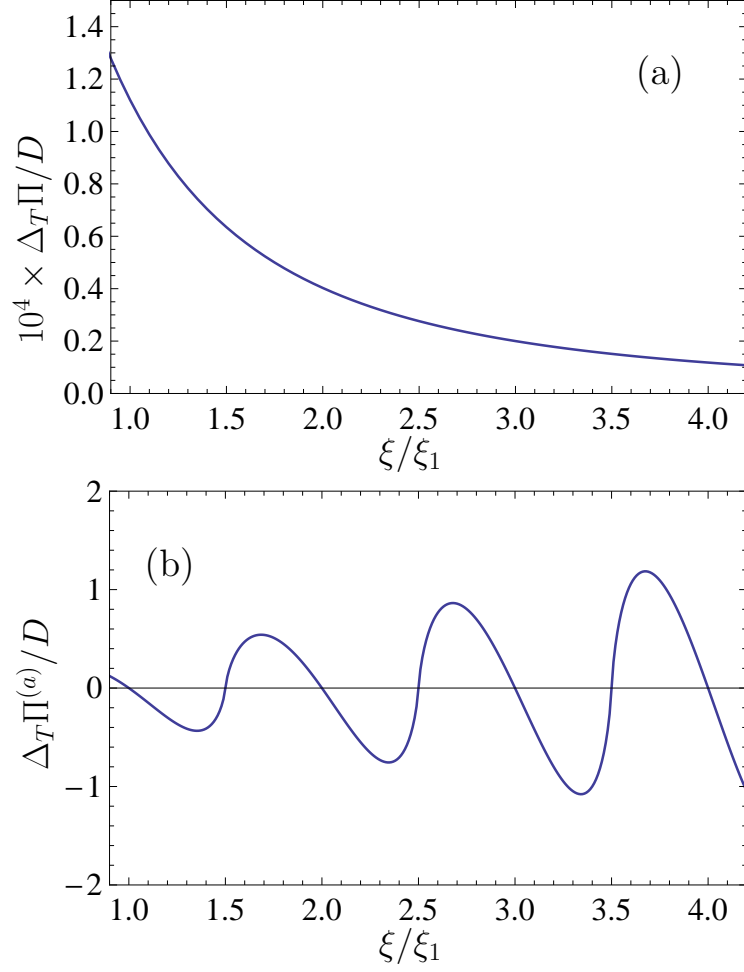


FIG. 2: (Color online) The normalized values of the thermal correction (47) to the combination of the components of polarization tensor of graphene computed as functions of imaginary frequency at $k_{\perp} = 10\xi_1$ (a) in this paper and (b) using the representation of Ref. [10].

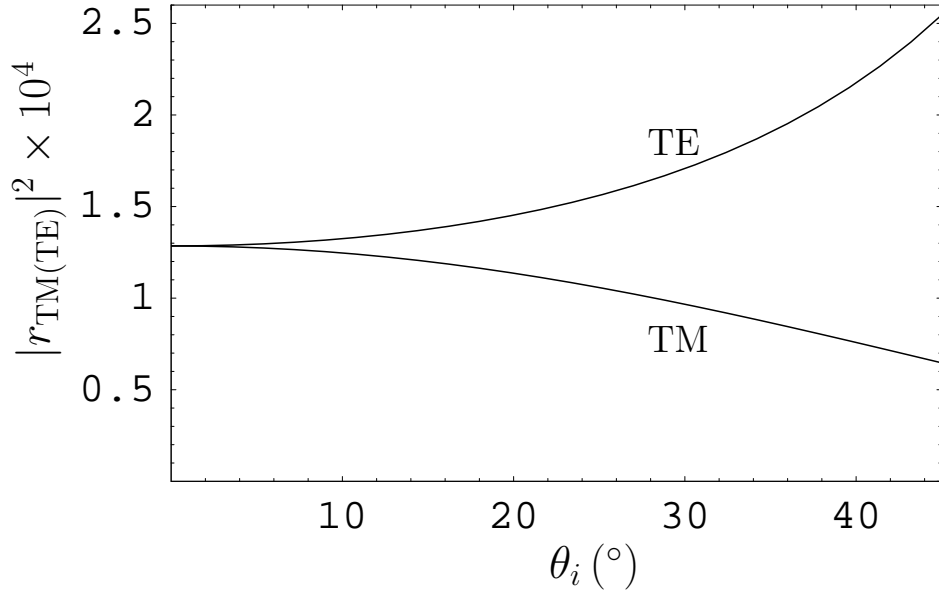


FIG. 3: Reflectivities of the TM and TE polarized light of high frequencies on graphene are shown as functions of the incidence angle by the lower and upper lines, respectively.

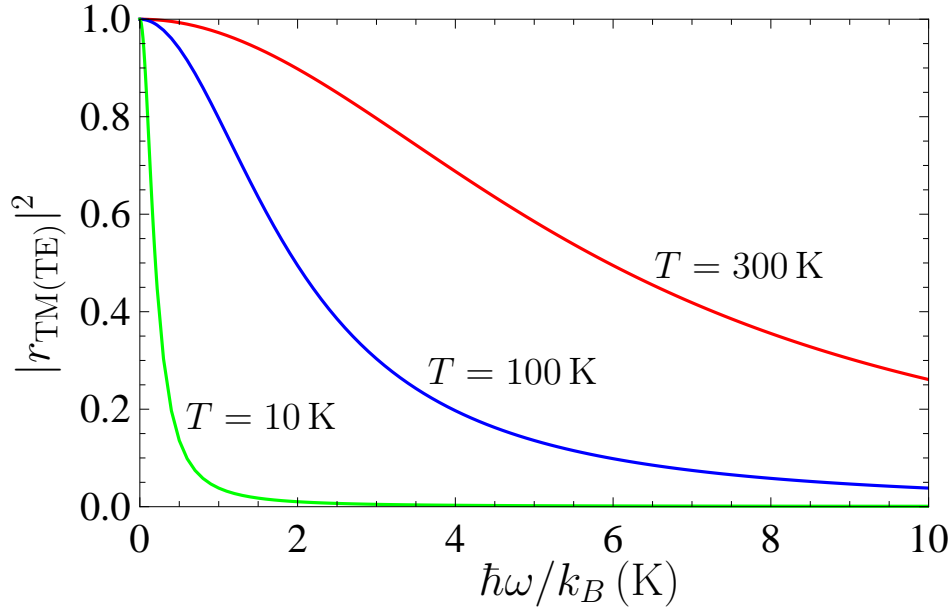


FIG. 4: (Color online) Reflectivities of graphene at the normal incidence at different temperatures $T = 10$ K, 100 K, and 300 K are shown as functions of frequency measured in K by the solid lines from bottom to top, respectively.

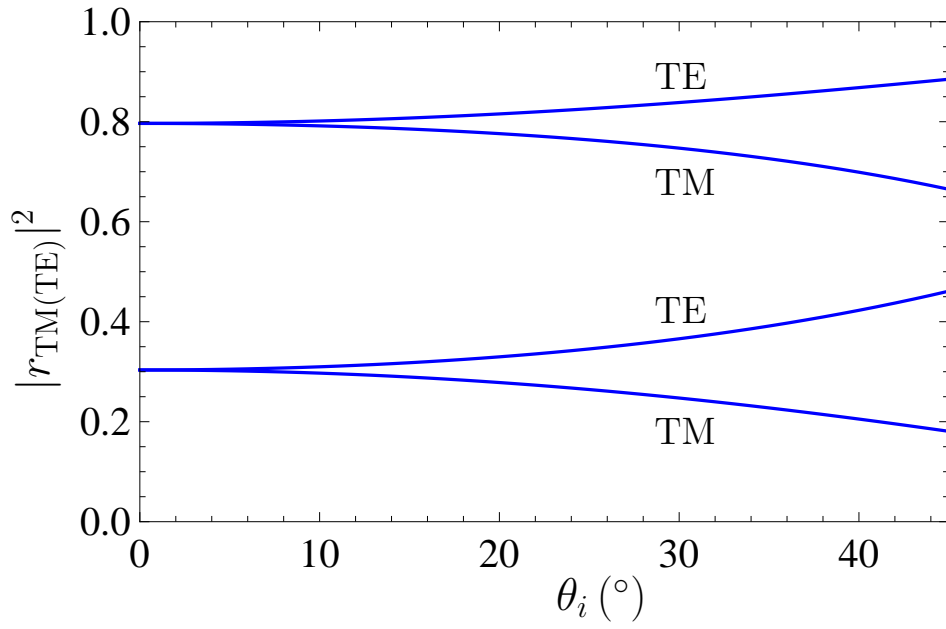


FIG. 5: (Color online) Reflectivities of the TM and TE polarized light of low frequencies ($\omega/T = 0.01$ and $\omega/T = 0.03$ for the upper and lower pairs of lines, respectively) on graphene are shown as functions of the incidence angle.

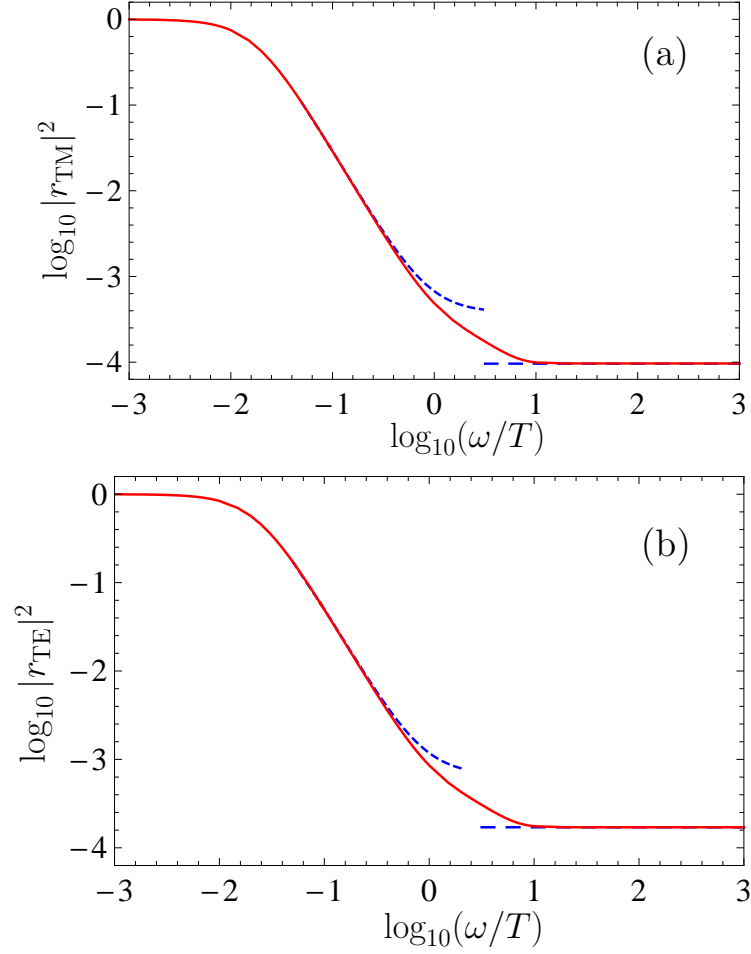


FIG. 6: (Color online) Reflectivities of the (a) TM and (b) TE polarized light on graphene are shown as functions of ω/T at the incidence angle $\theta_i = 30^\circ$. The solid, short-dashed and long-dashed lines are computed by the exact formulas, and by the asymptotic expressions for low and high frequencies, respectively.

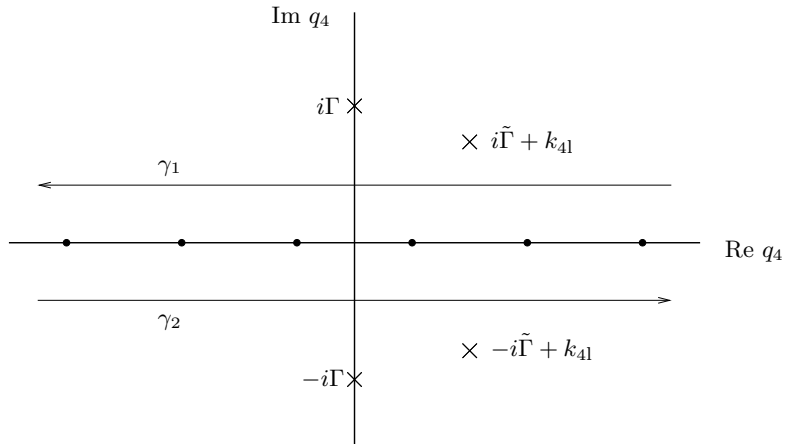


FIG. 7: The complex q_4 -plane containing the integration pathes γ_1 and γ_2 . The dots indicate the poles at the fermionic Matsubara frequencies and the crosses indicate four additional poles (see text for further discussion).